Observations of polymetallic Ag-Pb-Zn (± Au ± In) mineralization at the Eagle and Fisher vein-faults, airborne total field magnetics and identification of Tombstone age-equivalent aplite dykes in the Galena Hill area, Keno City, Yukon

***Dave Tupper*[1]**
Mega Precious Metals Inc.

***Venessa Bennett*[2]**
Yukon Geological Survey

Tupper, D. and Bennett, V., 2010. Observations of polymetallic Ag-Pb-Zn (± Au ± In) mineralization at the Eagle and Fisher vein-faults, airborne total field magnetics and identification of Tombstone age-equivalent aplite dykes in the Galena Hill area, Keno City, Yukon. *In*: Yukon Exploration and Geology 2009, K.E. MacFarlane, L.H. Weston and L.R. Blackburn (eds.), Yukon Geological Survey, p. 305-330.

ABSTRACT

We present a new dataset from the Eagle exploration project, completed in 2009 on the lesser explored southeast slopes of Galena Hill in the Keno Hill silver camp. The Keno Hill silver camp is hosted in Neoproterozoic and Paleozoic sedimentary rocks of the Selwyn Basin that were subsequently intruded by the Cretaceous Tombstone Plutonic Suite. Although a genetic association is documented between the Tombstone plutons and Au-As mineralization regionally, the genesis and age of the Keno Ag-Pb-Zn mineralization remains poorly understood.

Mineralization studied from the Eagle project area, while modally dominated by indium-rich sphalerite, was introduced in at least three distinct phases. A low-amplitude aeromagnetic high occurs at the southeast end of Galena Hill and is suggestive of a buried intrusion. Two new U-Pb age dates of *ca.* 93 Ma have been determined for aplite dykes, indicating the presence of Tombstone Suite intrusions within the Eagle property.

[1]*dt.pgeo@gmail.com*

[2]*venessa.bennett@gov.yk.ca*

INTRODUCTION

The Eagle Silver project of Mega Precious Metals Inc. (MPI; previously Mega Silver Corp.), is located on the southeast slope of Galena Hill in the Keno Hill silver camp, north-central Yukon (Figs. 1, 2). Total claim disposition comprises the Fisher, Eagle, Spiderman, Blue and One properties (Fig. 2). Exploration efforts by MPI during the past two years have focused on identifying economic extensions of both the Eagle and Fisher polymetallic vein-faults.

The mines of the Keno Hill silver camp, which included up to 35 different sites, produced a total 6 656 t (214 million ounces) of silver, 80% of which was extracted from veins located on the north slopes of Galena Hill (Cathro, 2006). Up to 45% of the total silver production was from the Hector-Calumet Mine alone, located on Galena Hill. The primary ore milled was galena-tetrahedrite-sphalerite-rich and averaged 1374 g/t (41.0 oz/ton) silver.

Although a genetic association between the mid-Cretaceous plutons of the Tombstone Suite and Au-As and W mineralization in the region (e.g., Scheelite Dome and Dublin Gulch) is well documented, the genesis and age of the Keno Ag-Pb-Zn mineralization remains poorly constrained. Lynch (1989) considered the Roop Lakes pluton, a member of the Tombstone Suite, to be the heat source linked to the concentration of the Keno Hill Ag-Pb-Zn mineralization, but not the source of the metals. Duncan Creek and its tributaries, parts of which drain the Eagle Silver project area (Fig. 2), have also produced a reported total of 15.5 million grams (49 416 oz) of Au

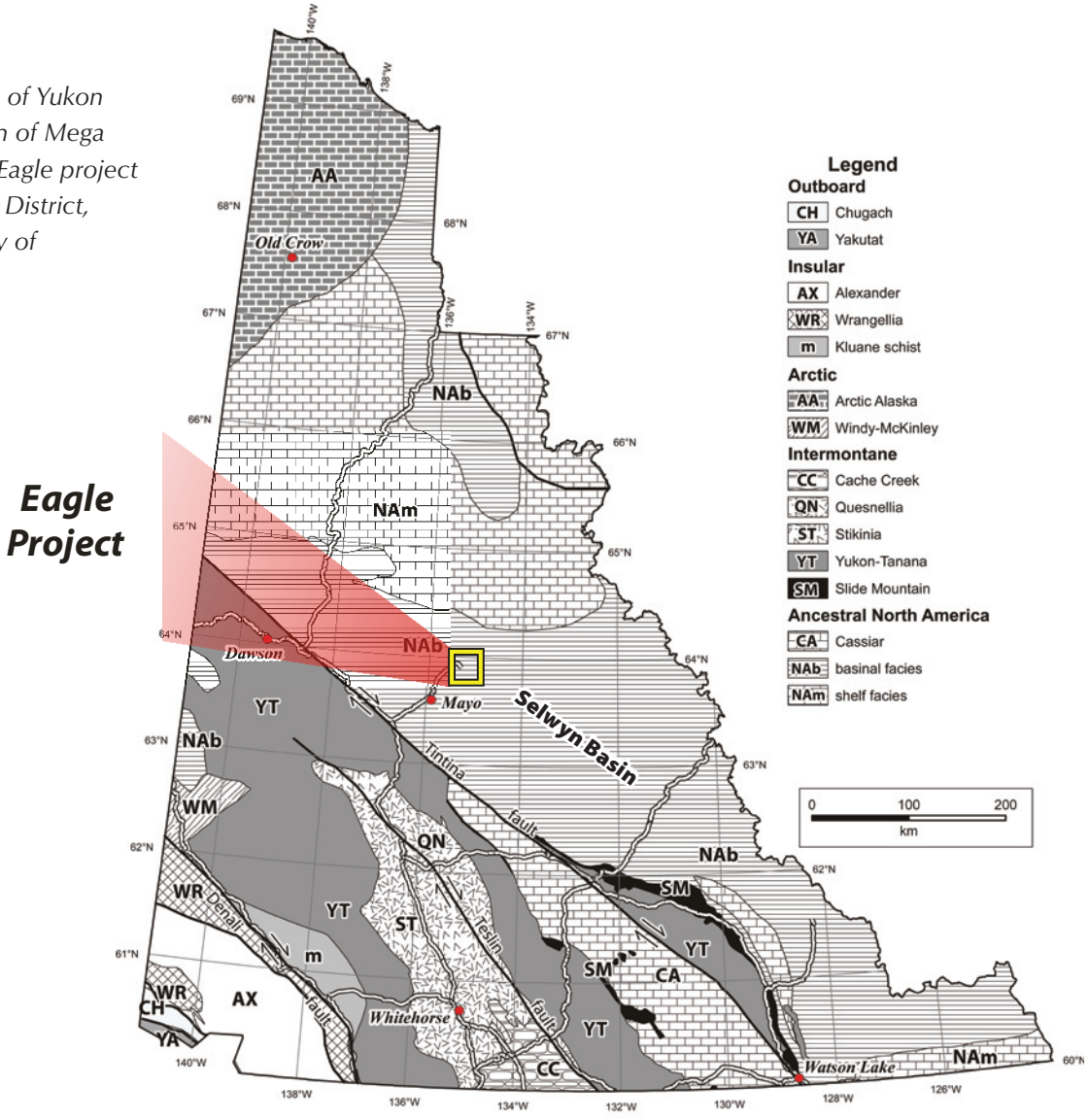

Figure 1. *Terrane map of Yukon illustrating the location of Mega Precious Metals Inc.'s Eagle project within the Keno Silver District, Selywn Basin (courtesy of M. Colpron).*

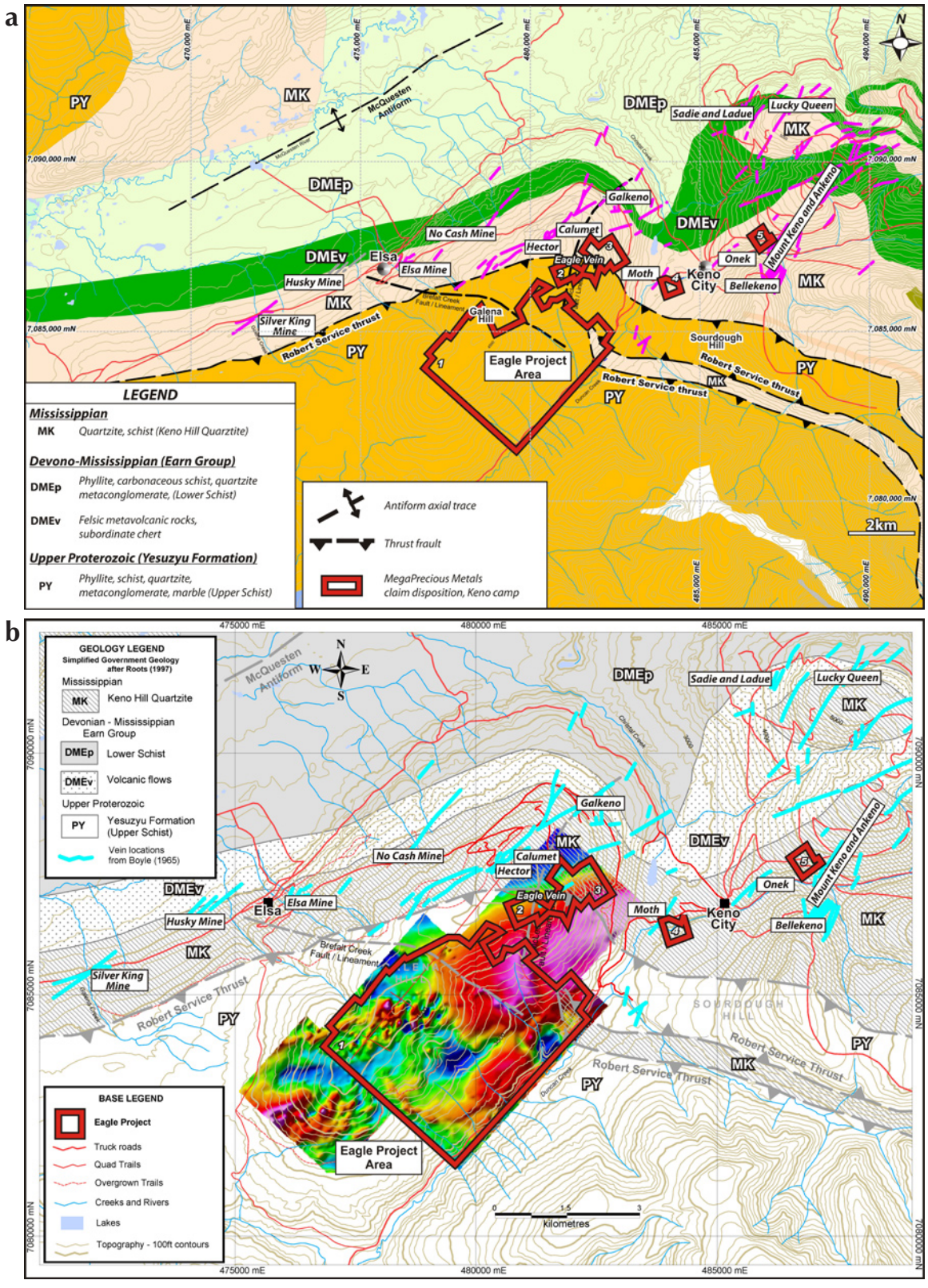

Figure 2. ***(a)*** *Geological map of Keno Hill camp illustrating the distribution of Ag-Pb-Zn properties and historic mines. The location of Mega Precious Metals Inc.'s claim disposition is outlined in red. Claim blocks labeled 1 – 5 represent Fisher, Eagle, Spiderman, Blue and One properties respectively.* ***(b)*** *Total magnetic intensity map acquired for Mega Precious claims superimposed on Keno Hill camp geological map.*

from 1898 to 2006 (LeBarge, 2007), indicating important bedrock reserves of Au exist within the Keno Hill silver camp.

In 2009, the Eagle Silver project was the focus of 4022 m of NTW diamond drilling targeting the Eagle Vein, a strong, steep southeast-dipping, vein-fault hosted within interbedded quartzite and phyllitic schist of the locally defined Keno Hill Quartzite. Vein intercepts of Ag-Pb-Zn-rich mineralization at Eagle and Fisher provide key petrographic observations that assist in the understanding of ore mineral paragenesis in this region of the Keno Hill silver camp. Mineralization observed in drill core from the Eagle Vein, although modally dominated by sphalerite, show at least three phases of mineralization including: (i) an early Au-enriched pyrite-marcasite-sphalerite ± cassiterite ± arsenopyrite phase associated with quartz-siderite gangue; (ii) an intermediate Ag-enriched galena ± chalcopyrite-pyrite ± stannite phase with overprinting late-stage siderite to cubic pyrite veining; and (iii) a late-stage, moderately Au-enriched pyrite ± arsenopyrite ± pyrrohotite ± cassiterite phase of mineralization that clearly overprints pre-existing Ag-Pb-Zn mineralization. Analytical results also indicate that the Eagle Vein includes potentially economic concentrations of indium with weighted average intercepts from hole D09-EE-07 containing over 3.1 m (from 217.8 to 220.9 m) of 3.55 g/t Au, 787.7 g/t Ag, 4.46% Pb, 18.68% Zn and 168.52 g/t In.

An aeromagnetic survey flown over the property provides additional information relevant to the question of its genesis. An elongate, low-amplitude aeromagnetic high occurs at lower elevations on the southeast end of Galena Hill and is unique within the Keno Hill silver camp (Figs. 2, 3). The geometrical expression of the anomaly is suggestive of a buried pluton, the margins of which

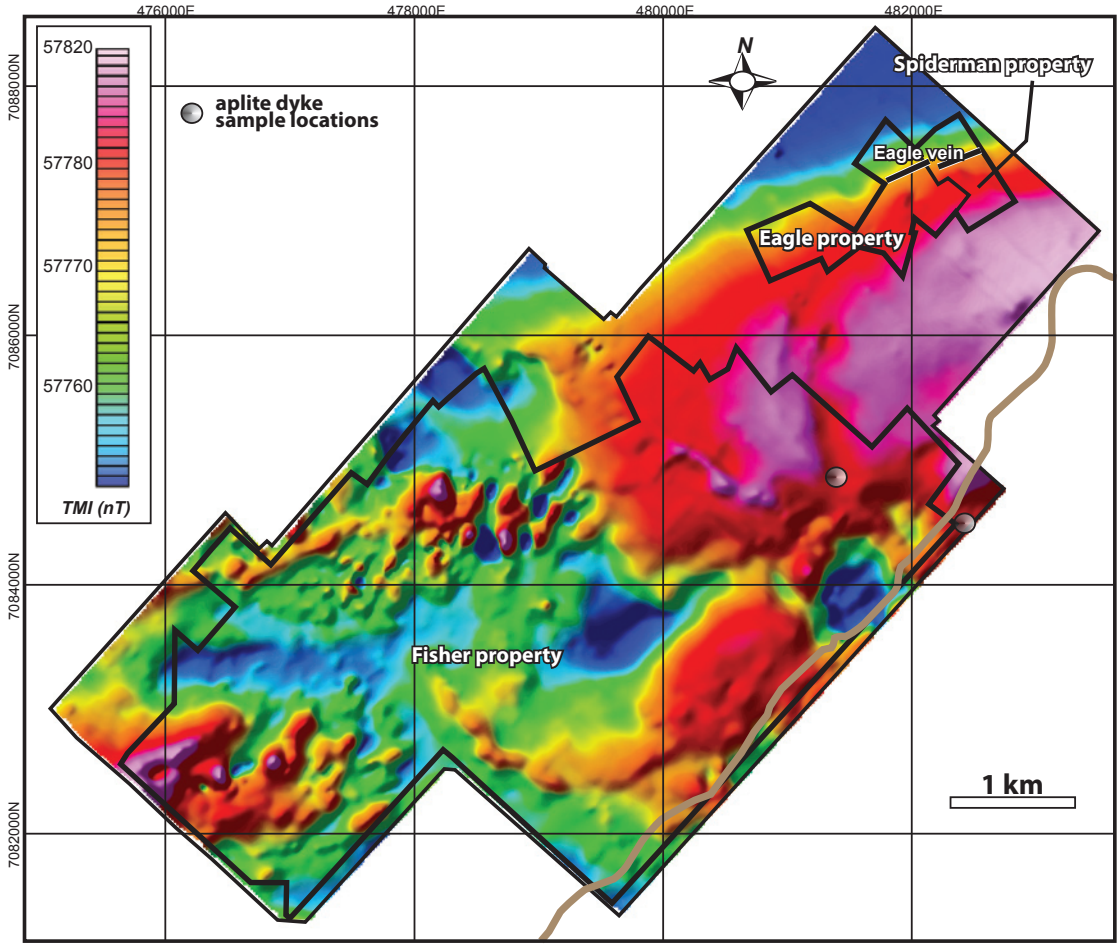

Figure 3. *Total magnetic field intensity map of Mega Precious Metals Inc.'s claim block, showing the locations of the Eagle, Fisher and Spiderman claims on edges of low-amplitude magnetic high. U-Pb geochronology sample locations marked.*

coincide with two proximal fault zones which separate the Eagle Vein from the prolific silver veins on the north slopes of Galena Hill (*i.e.*, Hector and Calumet). The age of this inferred intrusion is unknown; however, two new U-Pb dates on peripheral aplite dykes with similar texture and chemistry sampled from (i) within the Fisher fault zone, adjacent to the magnetic high, and (ii) to the south along Duncan Creek, are *ca.* 93 Ma, affirming the presence of Tombstone-age magmatism in the area.

REGIONAL GEOLOGY

The bedrock geology of the Keno Hill and surrounding Mayo area has been reported by Bostock (1947), Boyle (1956, 1957, 1965), McTaggart (1960), Kindle (1962), Watson (1986), Murphy (1997) and Roots (1997). The mineralogy and paragenesis of the Keno Hill silver base-metal veins have been discussed most extensively by Boyle (1956, 1957, 1965). Contributions have also been made by Franzen (1979), Lynch (1989; 2003), and Watson (1986). U-Pb geochronological data for intrusions in the area are reported in Roots (1997) and Murphy (1997). Sinclair *et al.* (1980), provided a K-Ar date for the mineralization from sericite of 90 Ma.

The Keno Hill camp is located within the Selwyn Basin of the northern Canadian Cordillera (Fig. 1). An informal tripartite stratigraphic subdivision has been applied to the highly deformed rocks of the camp during its protracted history; more recent work has shown that the succession is imbricated as well as highly deformed (Murphy, 1997; Roots, 1997; Fig. 2). The stratigraphically and structurally lowest informal unit of the camp is the 'lower schist' which is the local expression of the Devonian to Mississippian Earn Group (Fig. 2). In this area, the Earn Group comprises greenish-white, siliceous, chloritic-phyllitic schist (felsic metavolcanic), carbonaceous phyllite and minor quartzite horizons (Murphy, 1997). The Earn Group/'lower schist' is overlain by the Keno Hill Quartzite of Mississippian age (Mortensen and Thompson, 1990), a massive, clean, grey quartzite intercalated with lesser carbonaceous schist/phyllite. The structurally highest unit, the 'upper schist', is a composite unit disrupted by a cryptic regional thrust fault. The lower part of the 'upper schist' that directly overlies the Keno Hill Quartzite, comprises carbonaceous schist/phyllite, thin quartzite, and rare chloritic and quartz-sericite phyllite/schist of felsic metavolcanic protolith; all of the above is intercalated with dolomitic carbonate (Murphy, 1997; Roots, 1997; hereafter, the 'metavolcanic member'). The upper part of the 'upper schist' comprises quartz-mica schist, impure quartzite, muscovite-chlorite phyllite, grit, minor limestone and rare graphitic schist (Boyle, 1965; PY; Fig. 2); these rocks have now been correlated with the Yusezyu Formation of the Late Proterozoic to Cambrian Hyland Group. Tempelman-Kluit (1970) and Thompson (1995) recognized the older-over-younger relationship and placed the Robert Service thrust between the two parts of the 'upper schist'. The Earn Group, Keno Hill Quartzite and the lower part of the 'upper schist' were intruded by a number of Triassic (Mortensen and Thompson, 1990) gabbro sills that are historically referred to as greenstones; these typically exhibit a discontinuous, lenticular shape due to post-intrusion deformation (Murphy, 1997; Roots, 1997).

All lithological units in the Keno Hill area are isoclinally folded at a variety of scales, are significantly internally thrust imbricated, and have undergone greenschist-facies metamorphism (McTaggart, 1960; Roots, 1997). These structures are part of the Tombstone strain zone of Murphy (1997), the hanging-wall shear zone above the Tombstone thrust which places the deformed and metamorphosed Keno Hill succession to the northwest above less highly deformed strata, which is as young as Upper Jurassic. The Robert Service thrust is deformed within the Tombstone strain zone, attesting to its older age, and all structures are folded by the southwest-plunging McQuesten antiform (Murphy, 1997; Roots, 1997; Mair *et al.*, 2006).

All stratigraphic units of the region have been intruded by a post-deformation suite of granodiorite to quartz monzonite related to the Early to Late Cretaceous-age Tombstone Plutonic Suite. Medium-grained granodiorite of the Roop Lakes stock is located 20 km to the east and has a U-Pb titanite age of 92.8 ± 0.5 Ma (Roots, 1997). Intrusions of the *ca.* 63 – 69 Ma McQuesten Suite are also recognized in the region, where their emplacement locally exploited the existing structural weakness in the axis of the McQuesten antiform (Murphy, 1997).

The Elsa-Keno mining camp has been a major worldwide producer of silver from a series of sulphide-rich veins or vein-faults forming in dilational zones along east-northeast-striking, southeast-dipping, sinistral-oblique normal faults. Productive veins occur dominantly within the Keno Hill Quartzite, and to a lesser extent, in the underlying 'lower schist', although the host structures do extend up across the Robert Service thrust and into the structurally overlying Yusezyu Formation. Principal ore minerals include galena, sphalerite and tetrahedrite with

siderite and/or quartz as gangue material (Boyle, 1965). Cross-oriented vein faults, roughly perpendicular to the dominant structures, offset the mineralized structures (Boyle, 1965).

PROPERTY GEOLOGY

The southern slope of Galena Hill in the Eagle project area is underlain by the west-northwest-striking, moderate south-southwest-dipping structural succession of isoclinally folded/imbricated and unaltered to strongly altered Keno Hill Quartzite, the 'metavolcanic member' and Yusezyu Formation. The Keno Hill Quartzite is exposed only in the most northeastern part of the project area (Fig. 4). The surface traces of the contacts with the Yesuzyu Formation trend west-northwesterly across the gentle upper slopes of Galena Hill to the north.

The Keno Hill Quartzite is generally siliceous and has a variable thickness of 1-20 m. The unit is tan to pale grey, massive to laminated quartzite and medium to dark grey graphitic quartzite with centimetre to metre-scale, schistose graphitic partings, seams and interbeds. The Yusezyu Formation is a variable package of 1 to 10 m-thick horizons of grey schistose graphitic quartzite, dark grey graphitic schist, phyllitic schist and minor brown biotite schist, and pale grey marble. Green to pale green chlorite ± sericite ± talc schist of the 'metavolcanic member' occurs interspersed throughout all rock types within the zone between Keno Hill Quartzite and Yusezyu Formation.

Metagabbro lenses are intercalated with the Keno Hill Quartzite and the 'upper schist' contact zone where they vary from 0.5 m to 30 m in thickness and occur as competent green, variably foliated, sill-like bodies. They are calcareous, host trace amounts of chalcopyrite and commonly exhibit feldspar porphyry textures; the composition of these sill-like bodies are best described as foliated amphibolite (Boyle, 1965; Le Couteur, 2009). Greenstone units observed in the project area vary from weakly to intensely foliated and are characterized by pervasive chloritization, sausseritization and silicification.

Fine-grained, unfoliated grey-white, equigranular albite-quartz-muscovite-bearing aplitic dykes or sills were mapped just off the property to the southeast on Duncan Creek and in drill core (D09-EF-05) along the trace of the Fisher Creek fault on the Fisher property (Figs. 3, 4). Both localities were sampled for U-Pb geochronology.

The Eagle Vein trends 057º/60º southeast and has been traced laterally in outcrop and drillholes for up to 900 m along a southwest trend from the east boundary of the project area, as well as down dip for over 500 m (Fig. 4).

The McLeod-Fisher fault is a major structure that extends west-southwest from the Galkeno Mine, before arcing to the south into the Eagle project area along the trace of Fisher Creek (Fig. 4). Boyle (1957) shows that the McLeod fault, which is considered to post-date the Robert Service thrust, is a continuation of the McLeod Vein (azimuth 025º/60º southeast) at the Galkeno Mine. The McLeod-Fisher fault dips southeast to east-southeast and exhibits apparent left-lateral movement that structurally isolates the project area from the prolific silver-rich veins on the north slopes of Galena Hill. Additionally, the McLeod-Fisher fault is coincident with linear topographic features and linear aeromagnetic features interpreted from 2008 airborne total magnetics and magnetic tilt derivative survey plots completed by CMG Airborne (Figs. 3, 4). A second coincident topographic and geophysical lineament extends northwesterly from the headwaters of Duncan Creek, along the west tributary of Fisher Creek and over Galena Hill to align with the right-lateral Brefalt Creek cross-fault in the area of the Elsa Mine (Fig. 2). Right-lateral offsets in geology suggest that a similar north-trending, west-dipping structure extends north through the headwaters of Hinton Creek.

GEOCHEMICAL AND GEOPHYSICAL SURVEYS

Geochemical soil surveys completed in 2006 and 2008 by Mega Precious repeated historic surveys and delineated Pb-Zn-Ag-As anomalies that parallel the Eagle Vein system and the McLeod-Fisher fault (Figs. 4, 5). A 2008 geochemical soil survey on the Spiderman property defined a 450 m Ag-Pb-Zn anomaly extending east along strike from the Eagle Vein (Pb = 56 ppm and 4036 ppm). A second, east-trending, lower threshold (56 ppm to 122 ppm Pb) soil anomaly was also identified down slope to the south. Drilling in 2009 confirmed the presence of the Eagle vein-fault extending to the northeast, and also suggested that the source of the second anomaly to the south is associated with weakly mineralized chloritic schist and/or gabbro sill at approximately 100 m depth in the hangingwall to the Eagle Vein.

A 610 line-km airborne magnetic survey was completed for the entire Eagle Silver project area during 2008

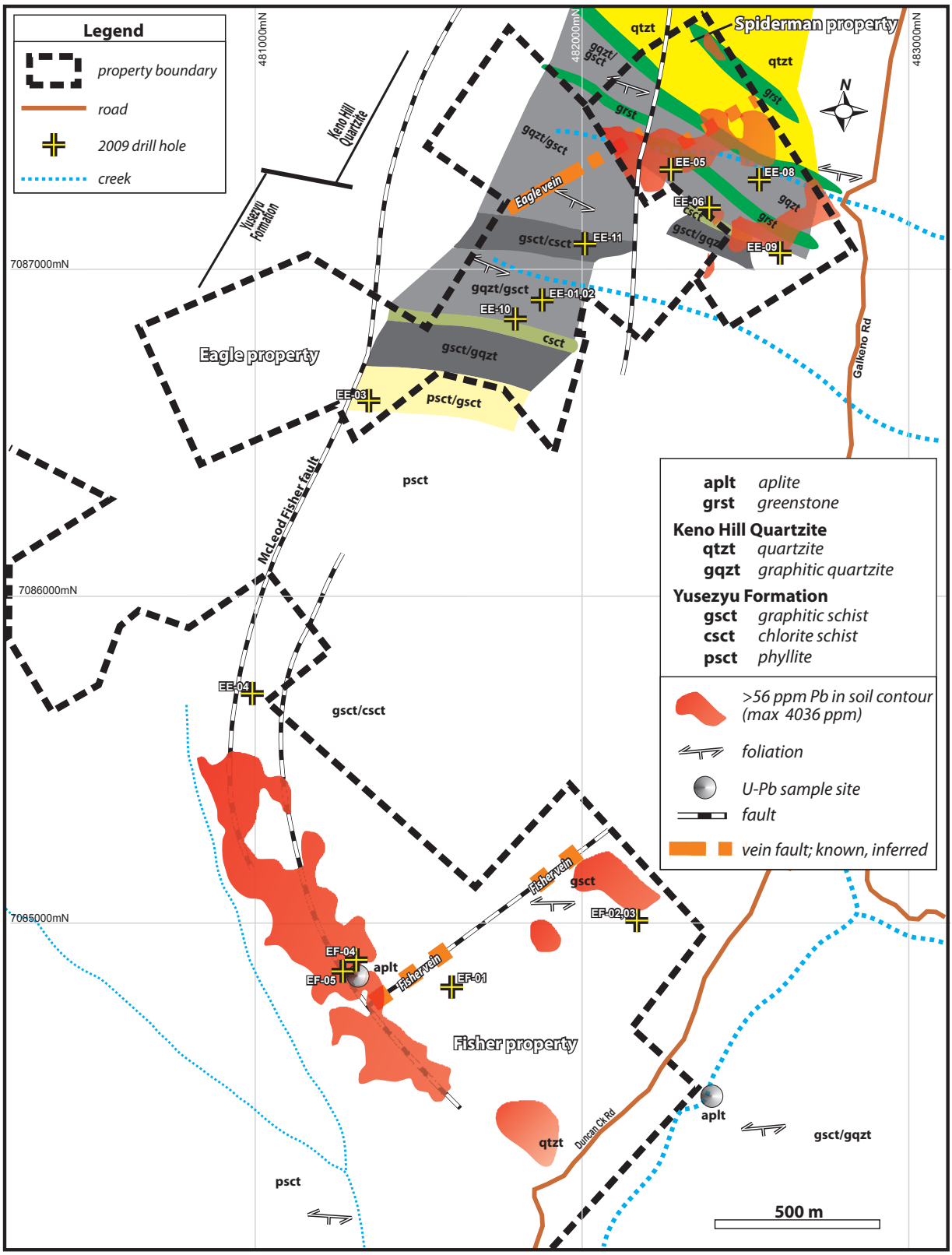

Figure 4. *Property-scale geological map for the Eagle project. The Eagle and Fisher veins, Pb-soil geochemical anomalies (>56 ppm) and U-Pb geochronology sample locations are marked.*

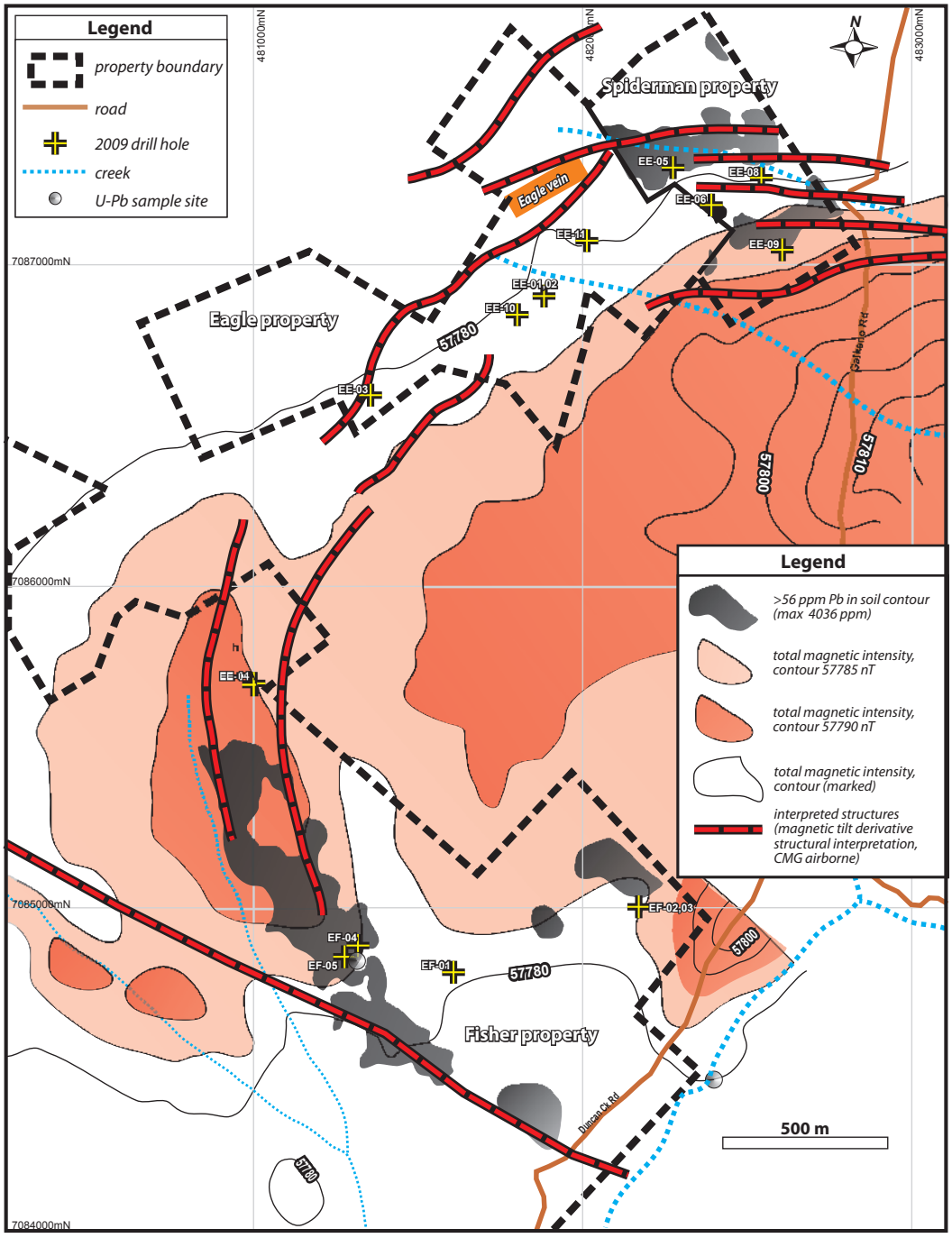

Figure 5. *Integrated Pb-soil geochemistry, simplified total magnetic field data and interpreted structures for the Eagle, Spiderman and parts of the Fisher properties. Surface projection of Eagle Vein and U-Pb geochronology samples are indicated.*

(Figs. 2b, 3, 5). Although resolution of the total field magnetic intensity anomaly is low (57707 to 57820 nT, TMI), the data indicate the presence of a west-southwest-trending, low-amplitude, elongate anomaly located immediately south of the Eagle Vein that may represent a buried intrusion. An arcing magnetic low extending through the main body of the anomaly is roughly coincident with the northward trend of the McLeod-Fisher linear, suggestive of magnetic destruction along a fault system. Linear features identified from magnetic tilt derivative analysis of the data suggest a number of arcuate structures that could be related to the interpreted buried intrusion (Scriven, 2008; Fig. 5).

MINERALIZATION

GENERAL OBSERVATIONS AND VEIN MORPHOLOGIES

The Eagle Vein represents the most significant mineral occurrence within the Eagle project area, with minor mineralization occurring within the Fisher fault zone. The Eagle occurrence is described by Boyle (1965) as being composed of two ladder vein-fault structures mineralized with siderite, quartz, massive pyrite, galena, sphalerite, arsenopyrite, freibergite, limonite and manganese oxides. Recent work confirms this, although no freibergite was observed, and the mineralogy is dominated by sphalerite -pyrite-marcasite. A variety of vein styles have been observed at Eagle (Fig. 6) and, apart from the sphalerite-dominant mineralogy, are generally consistent with classifications described by Watson (1986), including:

i. simple veins (D09-EE-07 and trench exposures) consisting of discontinuous bands and lenses of sulphides, with minor wall-rock brecciation present (Fig. 6a and b);

ii. breccia zones of matrix-supported (siderite-quartz-sulphide), angular to rounded quartzite breccia (D09-EE-02; Fig. 6c);

iii. sheeted zones of large angular blocks of country rock with gouge zones of siderite and massive sulphides (D09-EE-01 and -11);

iv. greenstone-hosted, narrow irregular veins of siderite and sphalerite occurring between parallel vein-faults (D09-EE-02, Fig. 6d);

v. zones of sheeted, narrow siderite stringer veins sub-parallel to the main vein structure, occurring within the vein-fault hangingwall (D09-EE-01, -09 and -11); and

vi. rare foliaform siderite-sphalerite-pyrite mineralization occurring subparallel to parallel to the main foliation plane within the schistose host rocks (Fig. 6e).

ORE MINERAL PARAGENESIS

Boyle (1965) outlines three principal paragenetic stages of ore mineralization associated with the formation of the Keno Hill Ag-Pb-Zn veins, including:

Stage 1: small quartz-carbonate stringers;

Stage 2: camp-wide quartz-pyrite-arsenopyrite-gold lenses developed in vein- faults; and

Stage 3: extensive series of vein-faults mineralized with siderite-pyrite-sphalerite-galena-freibergite lodes and minor quartz.

Macroscopic and petrographic observations (LeCoutour, 2009) of important mineralized vein intercepts from the Eagle Vein are broadly consistent with Boyle's (1965) sequence of silver and base-metal mineralization; however, mineralization occurring within the Eagle Vein is unique due to the ubiquitous breakdown of Stages 1 – 3 mineralization and subsequent replacement by prismatic pyrite-arsenopyrite-pyrrhotite, which is locally enriched in Au. Three main stages of mineralization are recognized for the Eagle Vein ore, including:

(i) early Au-enriched pyrite-marcasite ± sphalerite ± cassiterite ± arsenopyrite phase associated with a quartz-siderite gangue (Fig. 7a; 339 g/t Au);

(ii) intermediate Ag-enriched galena ± chalcopyrite-pyrite ± stannite mineralization which crosscuts early-phase sphalerite-siderite-marcasite and subsequently is crosscut by late-stage secondary siderite to cubic pyrite veining (Figs. 6, 7a-c); and

(iii) late-stage, moderately Au-enriched pyrite ± arsenopyrite ± pyrrhotite ± cassiterite phase of mineralization that clearly overprints pre-existing Ag-Pb-Zn mineralization (Fig. 8).

INDIUM MINERALIZATION

Iron-rich sphalerite in the Eagle Vein is highly enriched in indium where it is intergrown within the crystal lattice of coarse-grained sphalerite, combining with copper to replace zinc. High-grade zinc intercepts assayed 13.06% Zn and 182.80 g/t In over 10.9 m (*e.g.*, D09-EE-07, 210.5 to 221.4 m). No data are available from other veins in the region to suggest any zonation in indium levels of sphalerite; however, Boyle (1965) reports enrichment in indium in quartz-sericite schist in the camp. It is notable that the Eagle Vein occurs in the 'metavolcanic member' above the Keno Hill Quartzite where the sericite schists are particularly abundant.

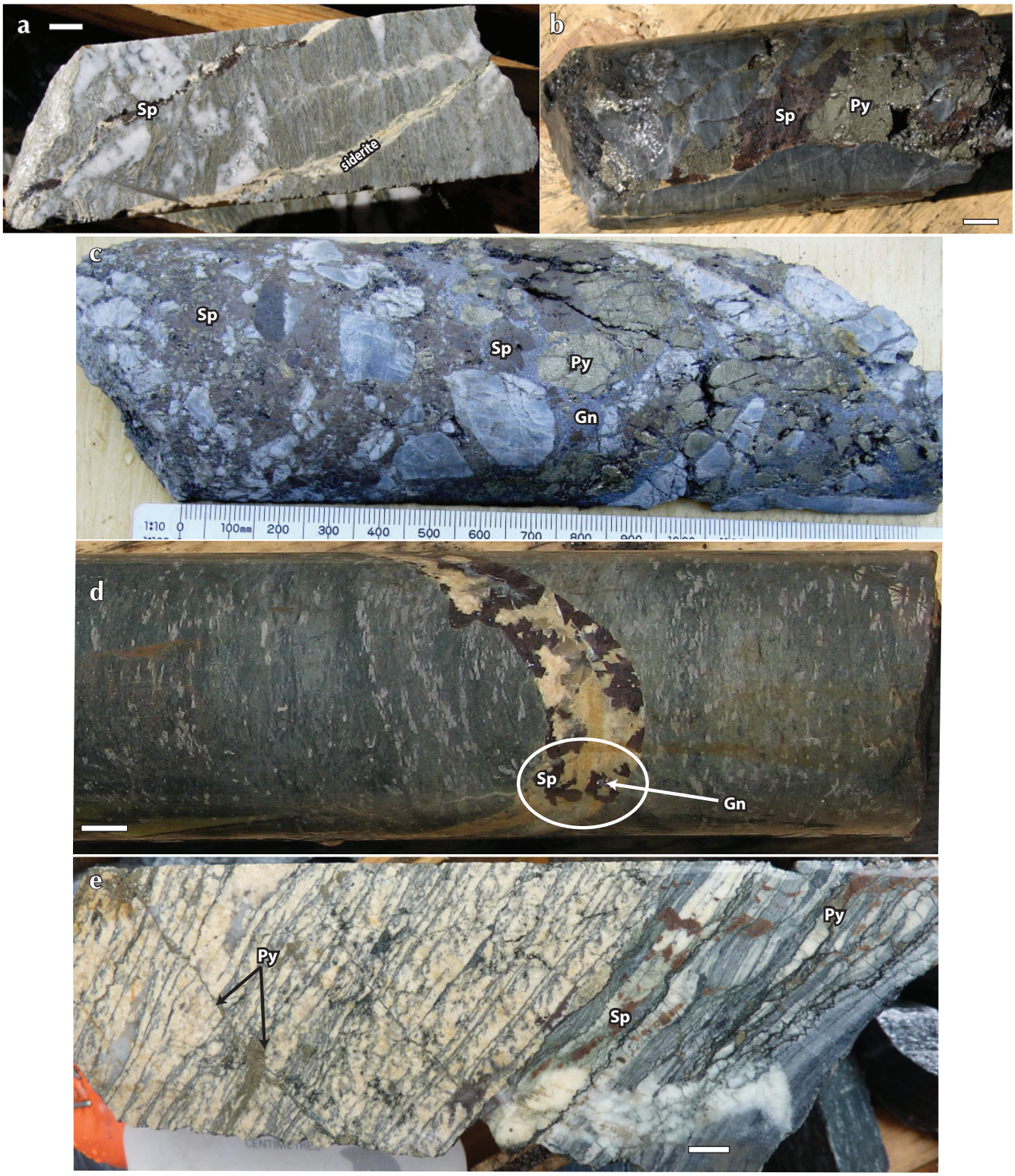

Figure 6. *Representative styles of base-metal vein mineralization from the Eagle and Fischer veins:* ***(a)*** *siderite-sphalerite vein crosscutting sericite-chlorite schist (D09-EE-01);* ***(b)*** *sphalerite-pyrite vein crosscutting massive quartzite (D09-EE-01);* ***(c)*** *sphalerite-galena-pyrite mineralization in breccia matrix, Fischer vein (D09-EE-02);* ***(d)*** *siderite-sphalerite ± galena vein crosscutting greenstone; and* ***(e)*** *foliaform siderite-sphalerite mineralization within quartz-sericite schist (D09-EF-03). Siderite-sphalerite mineralization crosscut by late, oblique pyrite vein. Sp = sphalerite, Gn = galena, Py = pyrite. Scale bars represent 1 cm.*

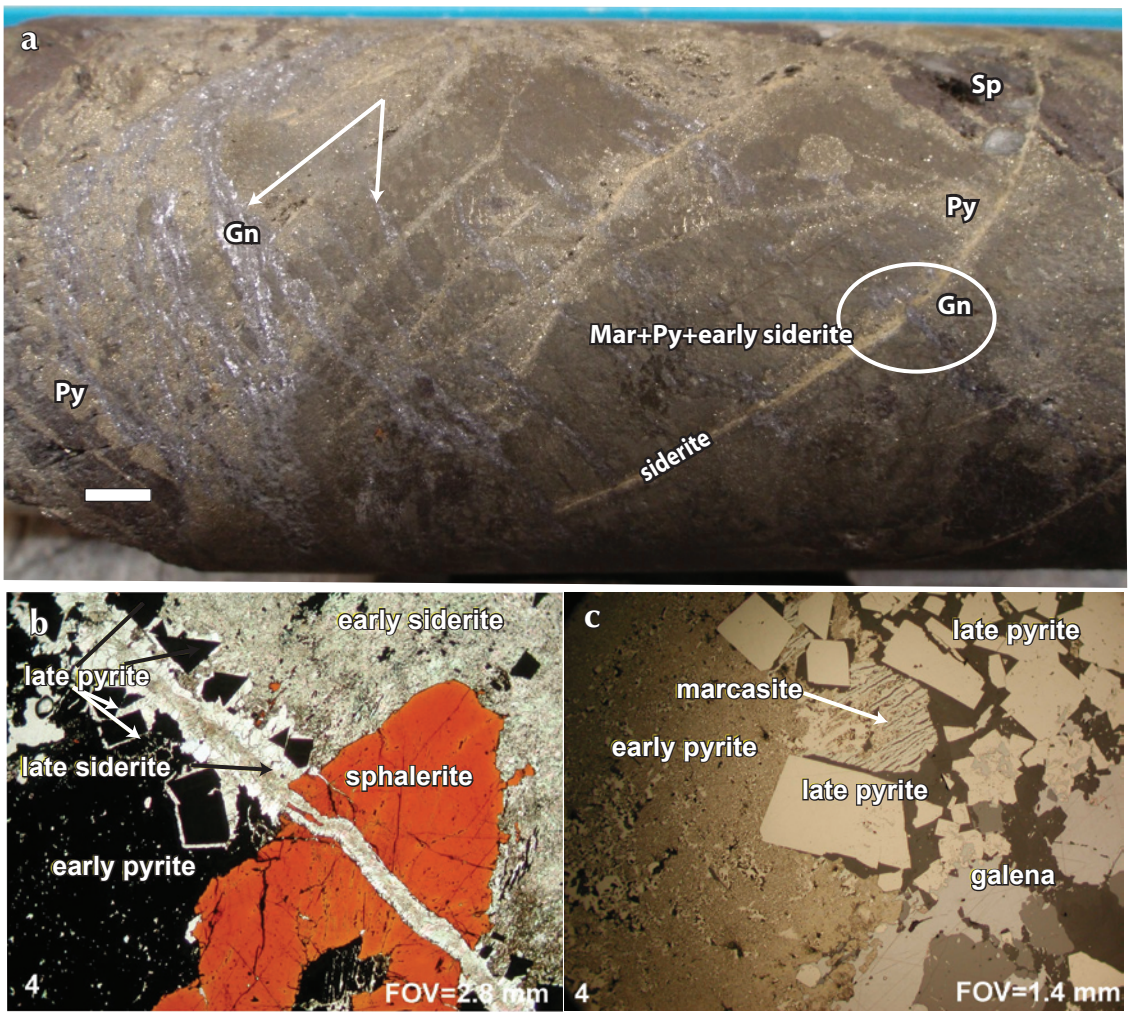

Figure 7. ***(a)*** *Early-stage polymetallic mineralization, Eagle Vein (339 g/t Au from 273.3-273.7 m, D09-EE-02). Note: Galena veins are latest phase of mineralization present. Scale bar represents 1 cm.* ***(b)*** *Early-phase sphalerite + siderite overprinted by siderite + cubic pyrite.* ***(c)*** *Early-phase pyrite + marcasite overprinted by (i) cubic pyrite (± siderite 2) and (ii) latest stage galena. Photomicrographs from LeCoutour (2009). Sp = sphalerite, Gn = galena, Py = pyrite, Mar = marcasite.*

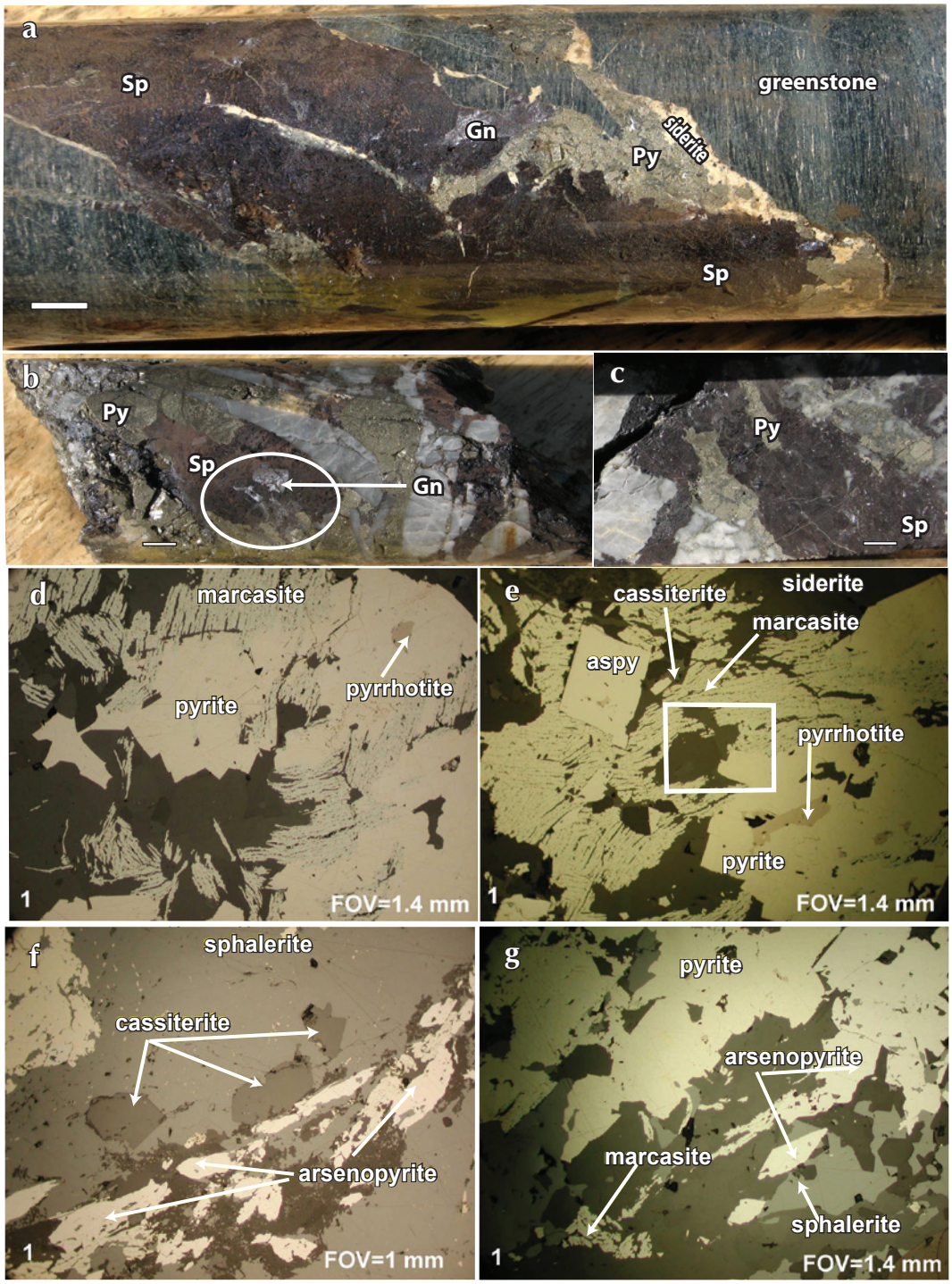

Figure 8. ***(a)*** *Sphalerite-siderite ± galena overprinted by pyrite in a vein crosscutting highly foliated greenstone, Eagle Vein (D09-EE-01);* ***(b)*** *sphalerite-galena infilling brecciated Keno Hill Quartzite and overprinted by late-stage pyrite, and* ***(c)*** *coarse-grained sphalerite replaced by secondary pyrite ± pyrrhotite. Reflected-light photomicrographs of sulphide textures within D09-EE-01, Eagle Vein. Scale bars represent 1 cm.* ***(d)*** *Early-phase marcasite overprinted by cubic pyrite intergrown with pyrrhotite;* ***(e)*** *early-phase marcasite-siderite overprinted by secondary prismatic arsenopyrite-cassiterite and cubic pyrite intergrown with pyrrhotite;* ***(f)*** *early-phase sphalerite overprinted by arsenopyrite ± cassiterite; and* ***(g)*** *late rhomboidal arsenopyrite-cubic pyrite overprinting early-phase marcasite intergrown with sphalerite. Photomicrographs from LeCoutour (2009). Field of view (FOV) marked. Sp = sphalerite, Gn = galena, Py = pyrite.*

SKARN/REPLACEMENT MINERALIZATION

Late-stage arsenopyrite-pyrite-gold skarn/replacement mineralization was encountered at depth within the Eagle Vein system (Fig. 9; D09-EE-01). The host lithology is a strongly deformed, brown sericite schist that is replaced by up to 45% coarse euhedral arsenopyrite and paramagnetic pyrite (Fig. 9b-d). The section assayed 1.23 g/t gold and was of interest as it was a new style of mineralization not encountered elsewhere on the property. Importantly, immediately above the

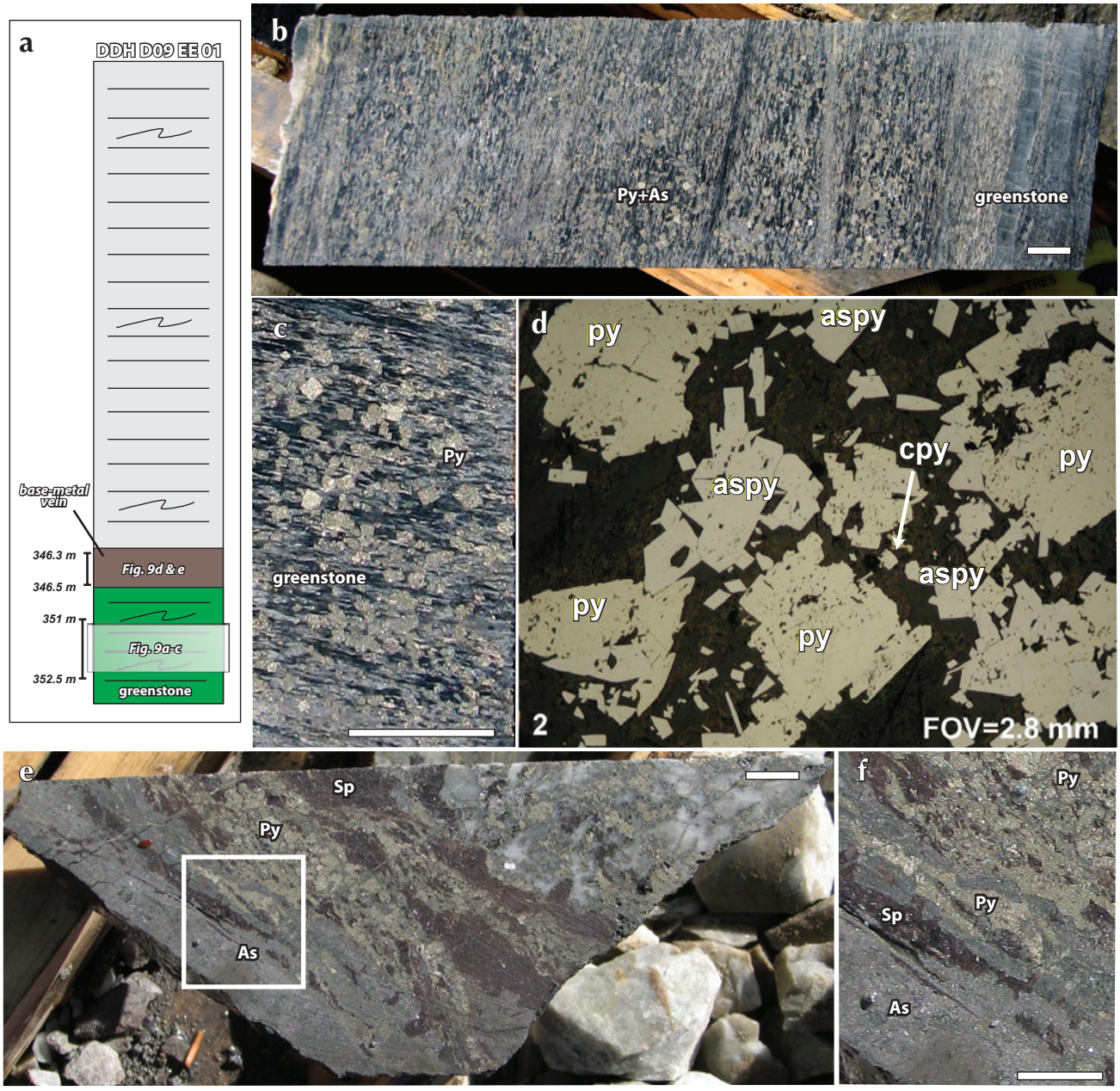

Figure 9. ***(a)*** *Schematic diagram illustrating mineralization at lower levels of D09-EE-01, 346.3 m to 352.5 m;* ***(b)*** *and* ***(c)*** *late post-deformational skarn/replacement-style mineralization overprinting highly foliated greenstone (1.2 g/t Au and 3841 ppm As; 351-352.5 m, D09-EE-01).* ***(d)*** *Reflected-light photomicrograph of gold-bearing late pyrite-arsenopyrite overprinting greenstone; field of view (FOV) marked; photomicrograph from LeCoutour (2009);* ***(e)*** *and* ***(f)*** *base-metal vein immediately overlying skarn/replacement pyrite-arsenopyrite mineralized zone. Early-phase sphalerite overprinted by pyrite and arsenopyrite (0.99 g/t gold and 6684 ppm As; 346.3-349.9 m, D09-EE-01). Scale bars represent 1 cm. Asp = arsenopyrite, Sp = sphalerite, Py = pyrite.*

replacement-style mineralized zone, more typical Ag-Pb-Zn mineralized veining occurred, which was characterized by early-phase sphalerite-siderite mineralization which is partially to completely replaced by pyrite-arsenopyrite (Fig. 9a, e and f). Assay results from this interval show elevations in Au and As, similar to the underlying replacement/skarn mineralized horizon, suggesting a genetic link between the Au-As mineralization in both horizons. The overprinting relationships are significant as they imply that the low-grade Au-As replacement/skarn-like mineralization, which is more typical of Tombstone intrusion-related Au-forming events in the region (*e.g.*, Gold Dome), overprints the Keno Hill Ag-Pb-Zn mineralizing event, which itself post-dates an early-stage strongly Au-enriched mineralizing episode.

GEOCHRONOLOGY

Two aplite dykes were located within the Eagle project area during surface mapping along Duncan Creek and drilling of the Fisher Vein. Both dykes were sampled for U-Pb dating to constrain the age of magmatism occurring within the Eagle Silver project area. Data collection using Laser Ablation Microprobe Inductively Coupled Plasma Mass Spectometry (LAM ICP-MS) techniques was completed in the Earth Sciences Department and the INCO Innovation Centre at Memorial University, St. Johns, Newfoundland. A detailed outline of the methodology is given in Bennett and Tubrett (this volume). Due to the prevalence of xenocrystic zircon within each of the dyke's zircon populations, an inherited zircon study was also completed for each sample. Analytical techniques to characterize the zircon populations included standard optical microscopy and backscattered electron (BSE) imaging and cathodoluminescence (CL) image analysis in order to permit greater understanding of zircon zoning and growth history. Image analysis was completed on all zircon grains selected (n = 20 – 80 depending on yield). Field relationships and zircon zonation styles are briefly described for each sample before reporting the U-Pb isotopic results. Final interpreted crystallization ages are based on calculation of concordia ages from individual U-Pb isotopic analyses that have a probability of concordance greater than 0.20 (see Bennett and Tubrett, this volume for more information on data treatment). Weighted-mean $^{206}Pb/^{238}U$ ages are also reported to remain consistent with current U-Pb geochronology reporting trends. Uncertainties reported for all calculated ages and plotted on associated concordia and weighted mean diagrams are at the 2σ uncertainty level, unless stated otherwise. Final age calculations include U decay-constant uncertainties which are plotted graphically on concordia plots. Concordia and weighted mean $^{206}Pb/^{238}U$ ages were calculated as per Ludwig (1999). The concordia age that includes U decay-constant uncertainties is considered the best estimate of the crystallization age of a sample. Where a concordia age has a mean square of weighted deviates (MSWD) >1.5, the weighted mean $^{206}Pb/^{238}U$ age is considered the best estimate of the crystallization age. Magmatic rims were analysed using a 10 µm-diameter line raster. All inherited zircon analyses were completed using the standard 40 x 40 µm box raster (see Bennett and Tubrett, this volume). Uranium and Th concentration data and Th/U ratios were also calculated for each sample and are reported in Appendices 1 – 4.

FISHER VEIN APLITE (D09-EF-05)

During drill testing of the Fisher fault zone, an ~3 m (apparent width) aplitic dyke with brecciated upper and lower contacts was intersected from 36.0 m to 39.3 m depth in D09-EF-05 (Fig. 10a). The aplitic dyke has a fine-grained, saccharoidal texture and consists of subequal amounts of quartz and feldspar and approximately 20% - 25% biotite and muscovite. Weak to moderate chlorite-epidote alteration is pervasive throughout the intrusive unit where intersected in D09-EF-05.

Approximately 55 zircon grains of poor to moderate quality were liberated from the aplitic dyke sampled from the Fisher fault zone (Fig. 10c). Inherited zircon, in the form of both visible cores and grains with widely varying optical features (*e.g.*, grain shape, colour and inclusions), makes up the majority of zircons present in this sample. The grains selected for analysis were grossly subdivided into: (i) subrounded to rounded zircons varying from dark pink turbid grains to translucent, inclusion-free grains; and, (ii) elongate, sub-prismatic grains with thin, inclusion-free, translucent rims. One prismatic and translucent needle fragment was also identified and selected for analysis.

Backscattered electron (BSE) and cathodoluminescence (CL) image analyses were completed on all zircon grains sampled. Representative images are given in Figure 11. Image analysis supports the initial interpretation based on optical criteria that the greater majority of zircons represent an inherited population. No single uniform zonation style was recognized amongst the inherited grains suggesting multiple sources for the inherited zircon (Fig. 10b). Importantly, four zircon rims were

characterized by very bright BSE and CL responses, suggestive of high U and/or Hf concentrations (Fig. 11a). Where rim development was more significant, oscillatory zoning is observed (Fig. 11aiii). Similarity of BSE/CL responses of these rims and occurrences of rim oscillatory zoning (where better developed) suggests that new magmatic zircon growth associated with the aplitic magma was restricted to rim development on favourable inherited nuclei.

Four analyses were collected from the rims described above (Appendix 1). A concordia age calculated from these rim analyses yielded an age of 93.6 ± 1.4 Ma (MSWD = 2.7) and a weighted mean $^{206}Pb/^{238}U$ age of 93.3 ± 1.4 Ma (MSWD = 0.78; Fig. 12a and b). Concentration data calculated from magmatic rim analyses ranges from 3243 ppm to 4874 ppm U and 85 ppm to 131 ppm Th (Appendix 1) and demonstrates the U-rich nature of the magmatic rims. Twenty-two zircon cores were analysed to assess sources of inheritance

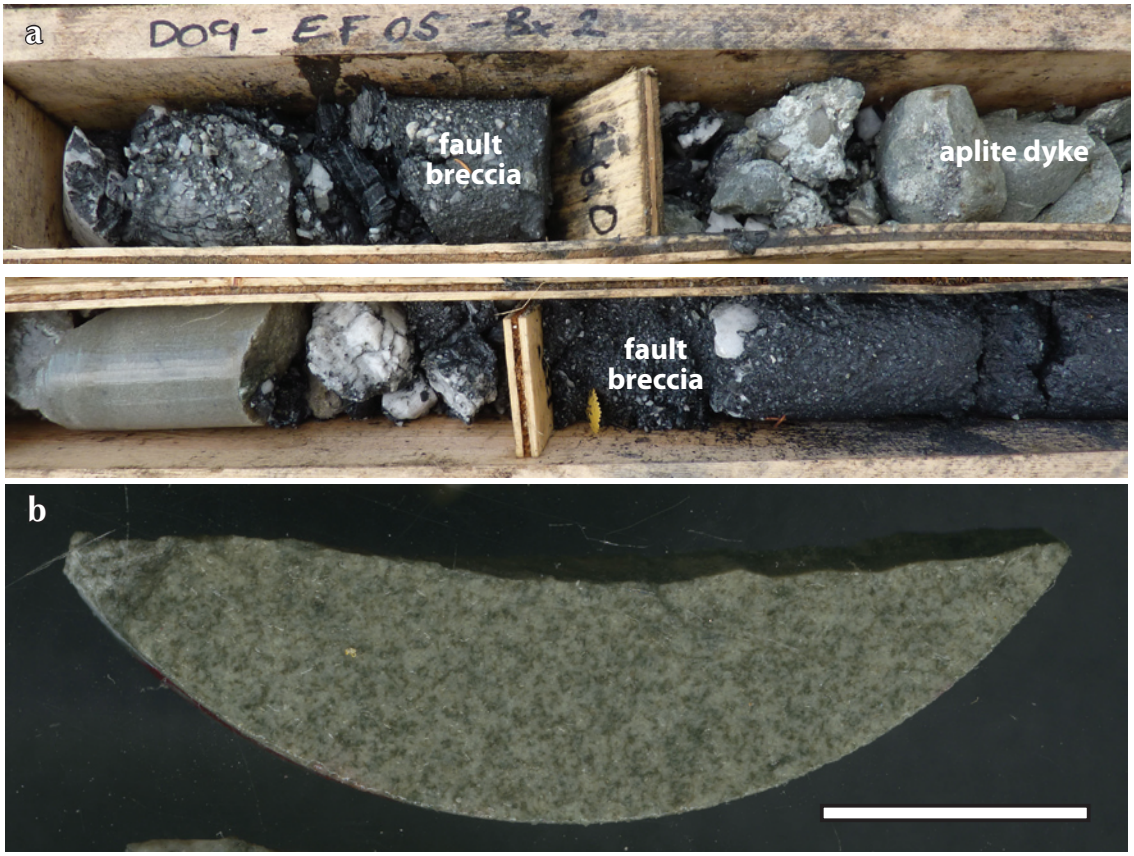

Figure 10. ***(a)*** *Core photo of brecciated upper and lower contacts of aplite dyke sampled from D09-EF-05 (within Fisher fault zone) for U-Pb age dating;* ***(b)*** *slab image of the aplite dyke. Scale bar represents 1 cm.* ***(c)*** *Transmitted-light images of zircon grains extracted from the aplite dyke. Scale bar represents 50 μm.*

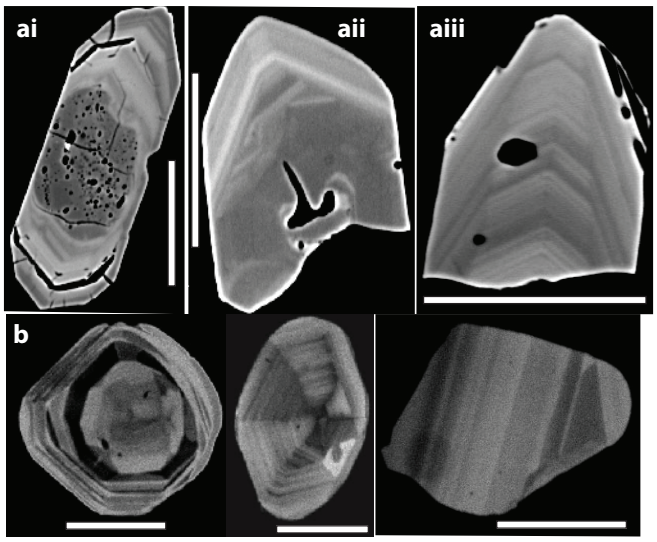

Figure 11. ***(a)*** *BSE images of magmatic zircon extracted from aplite dyke sampled from D09-EF-05. Magmatic zircon occurs as overgrowths on xenocrystic cores (11ai and aii) or as fine-grained needles or needle tips (11aiii);* ***(b)*** *CL images of inherited zircon grains. All scale bars represent 50 µm. BSE = backscattered electron, CL = cathodoluminescence.*

within the aplite sample (Appendix 2). Several inherited populations are recognized in the sample, which range in age from *ca.* 405 Ma to 2805 Ma within important Mesoproterozoic (*ca.* 1000 Ma, 1255 Ma, 1380 Ma, 1410 Ma and 1580 Ma), Paleoproterozoic (1720 Ma, 1750 Ma, 1905 Ma, 1955 Ma and 2005 Ma) and Neoarchean populations (2555 Ma, 2660 Ma and 2805 Ma; Figs. 12c and 13a). Th/U ratios calculated for all analyses clearly illustrate the difference between magmatic and inherited zircon chemistry (Fig. 13b).

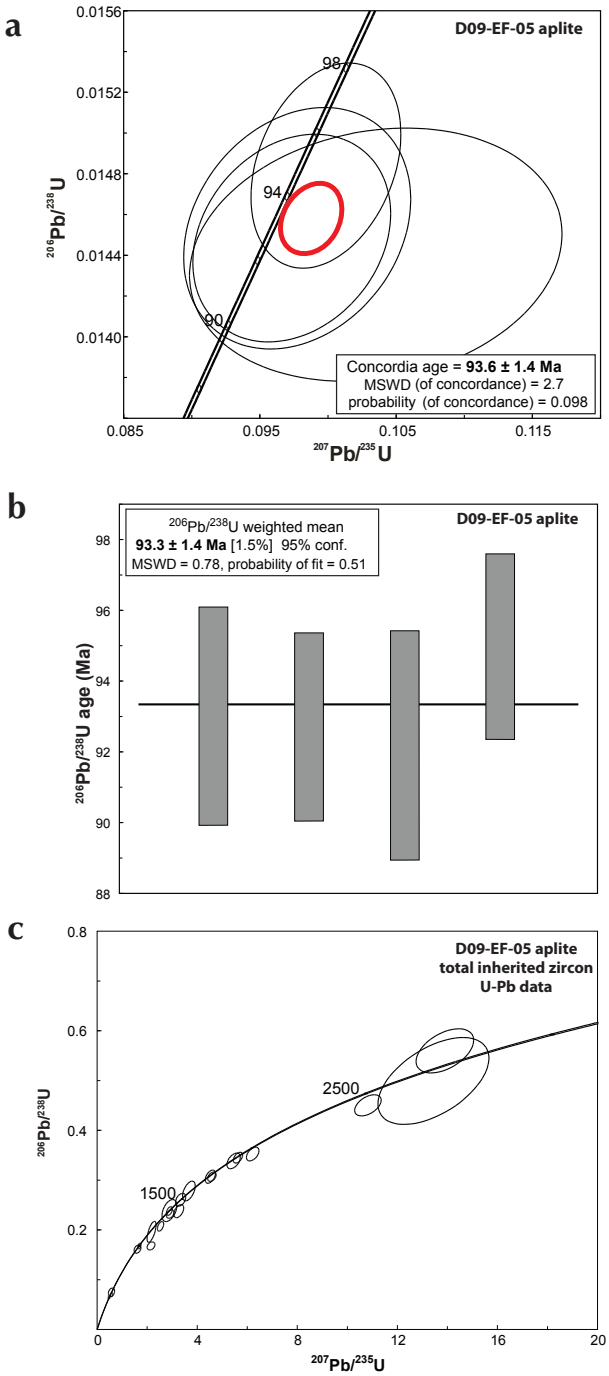

Figure 12. ***(a)*** *Concordia diagram for U-Pb LAM ICP-MS analyses of magmatic zircon from aplite dyke, D09-EF-05.* ***(b)*** *Plot of weighted mean $^{206}Pb/^{238}U$ ages of magmatic zircon from aplite dyke, D09-EF-05.* ***(c)*** *Concordia diagram for U-Pb LAM ICP-MS analyses of inherited zircon from aplite dyke, D09-EF-05. Notes: 1. On all diagrams MSWD = mean square of the weighted deviates. 2. On all U-Pb concordia diagrams, data point error ellipses represent 2σ error and 2σ uranium decay constant errors are included in final age calculation. 3. On all weighted mean $^{206}Pb/^{238}U$ diagrams, box heights represent 2σ.*

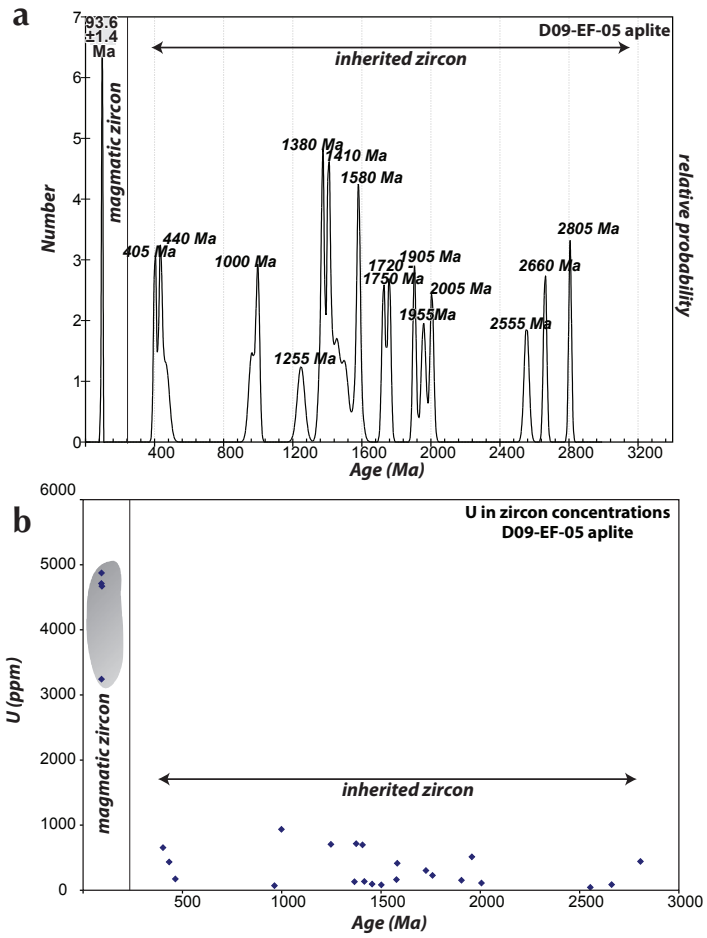

Figure 13. (a) *Cumulative probability diagram illustrating the distribution of inherited zircon populations in aplite dyke sampled from D09-EF-05. Crystallization age plotted for reference.* ***(b)*** *U concentration vs.age for all zircon populations within the aplite dyke. Magmatic zircon is distinctive in high U concentrations when compared to the inherited populations (≤1000 ppm).*

DUNCAN CREEK APLITE

A second aplitic dyke of similar texture and mineralogy to that observed in D09-EF-05 was mapped at surface on the northeast side of Duncan Creek where it intrudes graphitic schist and laminated quartzite of the 'upper schist' (482495E 7084445N; Figs. 3-5; Fig. 14a and b). The dyke is approximately east-trending and dips south, and is concordant to locally discordant to the prevailing foliation within the host 'upper schist'.

The sample yielded abundant zircons of highly variable quality which appeared similar in appearance to zircon populations in the aplitic dyke sampled from the Fisher fault zone. A greater zircon yield allowed for improved optical subdivision of the zircon populations into three main populations including: (i) irregular grains with core and rim zircon growth; (ii) subrounded to sub-prismatic zircon varying from dark pink turbid grains to translucent, inclusion-free grains; and (iii) a minor population of translucent, prismatic needles (Figs. 14c - e).

Backscattered electron and CL imaging of zircons selected from all three populations indicates that inherited zircon populations dominate (Fig. 15), as was the case for the aplite dyke sampled within the Fisher fault zone. Magmatic zircon occurs as bright BSE/CL rims, and more rarely as oscillatory zoned needles (Fig. 15a).

Eleven analyses were collected from rims and needles described above (Appendix 3). A concordia age calculated from magmatic zircon yielded an age of 93.6 ± 0.9 Ma (MSWD = 0.34) and a weighted mean $^{206}Pb/^{238}U$ age of 93.5 ± 1.2 Ma (MSWD = 1.3; Fig. 16a,b). These ages are virtually identical to those determined for the aplitic dyke occurring within the Fisher fault zone. Concentration data calculated from magmatic zircon vary from 612 ppm to 8502 ppm U and 54 ppm to 1248 ppm Th (Appendix 3). Forty-two zircon cores were analysed to assess sources of inheritance within the aplite sample (Fig. 16c; Appendix 4). Inherited populations range in age from *ca.* 265 Ma to 2660 Ma. Four concordant points for the youngest inherited zircon population yield a concordia age of 266 ± 3.8 Ma (MSWD = 0.65; Fig. 16d). Other inherited ages in the Duncan Creek aplite are similar to those determined for the Fisher fault aplite. Important inherited populations are Silurian (*ca.* 430 Ma), Mesoproterozoic (*ca.* 1010 Ma, 1160 Ma and 1350 Ma), Paleoproterozoic (1630 Ma, 1700 Ma, 1760 Ma, 1870 Ma and 1920 Ma) and Neoarchean (2640 Ma and 2660 Ma; Figs. 16c and 17a). Th/U ratios calculated for all analyses illustrate the difference between magmatic and inherited zircon chemistry (Fig. 17b).

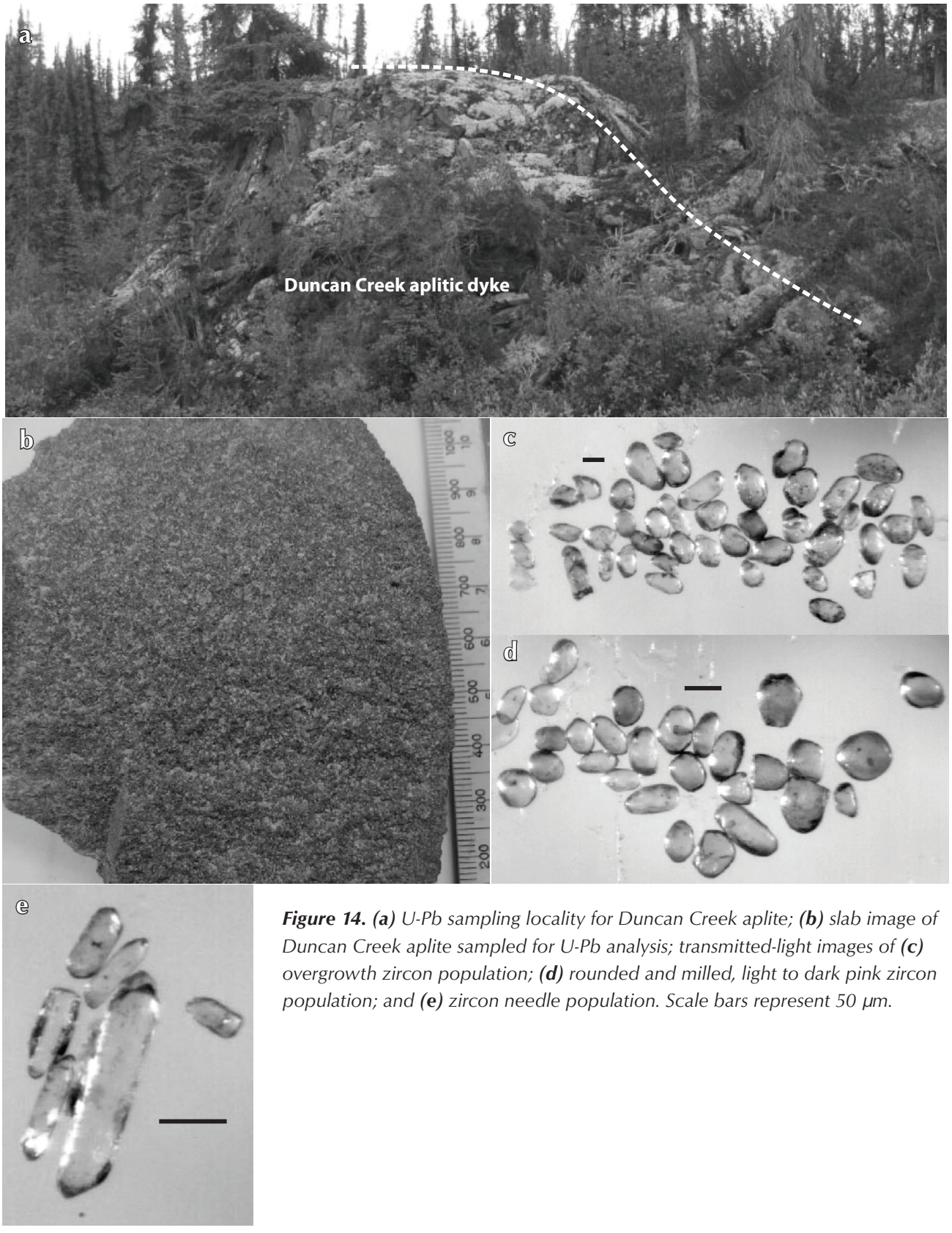

Figure 14. *(**a**) U-Pb sampling locality for Duncan Creek aplite; **(b)** slab image of Duncan Creek aplite sampled for U-Pb analysis; transmitted-light images of **(c)** overgrowth zircon population; **(d)** rounded and milled, light to dark pink zircon population; and **(e)** zircon needle population. Scale bars represent 50 µm.*

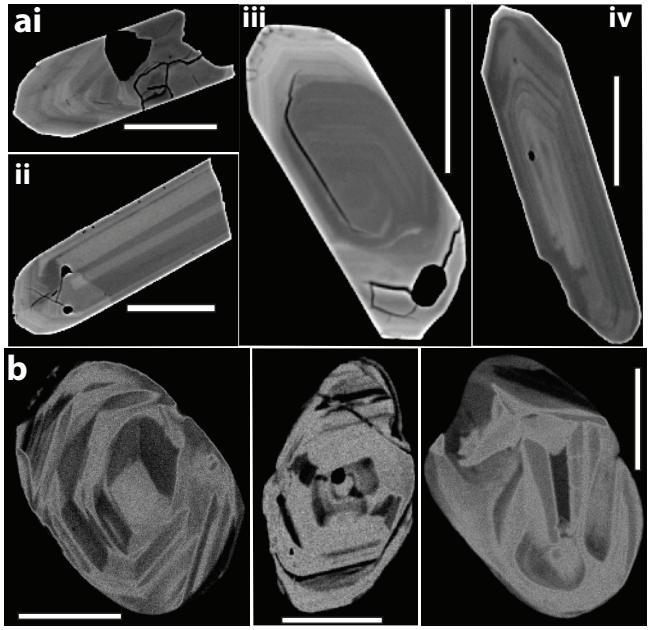

Figure 15. ***(a)*** *BSE images of magmatic zircon from Duncan Creek aplite. Magmatic zircon occurs as overgrowths on xenocrystic cores (15ai-aiii) or as fine-grained needles (15aiv).* ***(b)*** *CL images of inherited zircon grains. All scale bars represent 50 µm. BSE = backscattered electron, CL = cathodoluminescence.*

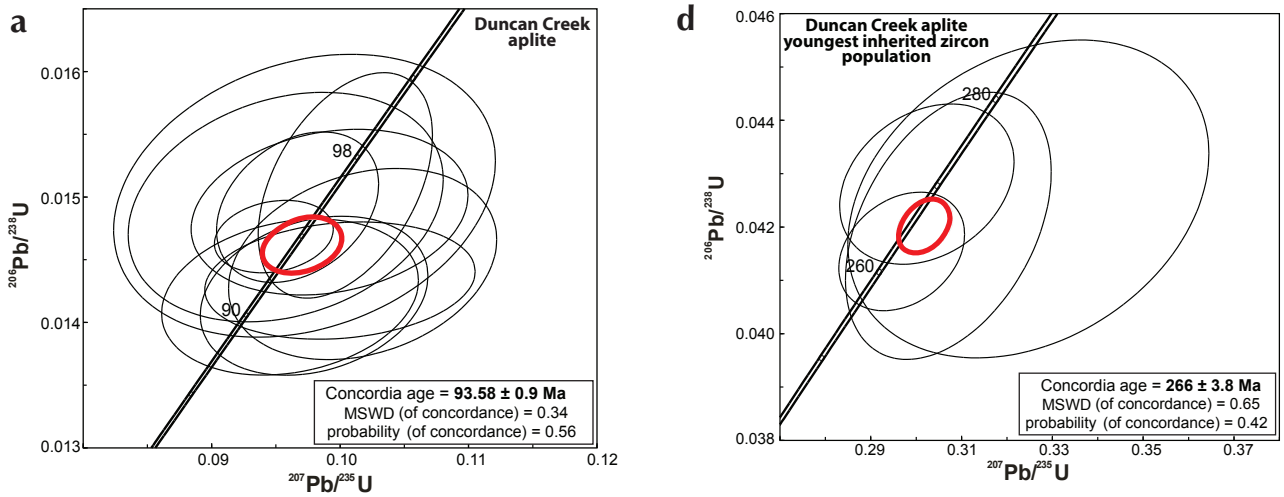

Figure 16. ***(a)*** *Concordia diagram for U-Pb LAM ICP-MS analyses of magmatic zircon from Duncan Creek aplite. Individual analyses with probability of concordance less than 0.2 are not included in final data calculations.* ***(b)*** *Plot of weighted-mean $^{206}Pb/^{238}U$ ages with probability of concordance greater than 0.20.* ***(c)*** *Concordia diagram for U-Pb LAM ICP-MS analyses of inherited zircon from Duncan Creek aplite.* ***(d)*** *Concordia diagram for U-Pb LAM ICP-MS analyses of youngest inherited zircon population (ca. 266 Ma).*

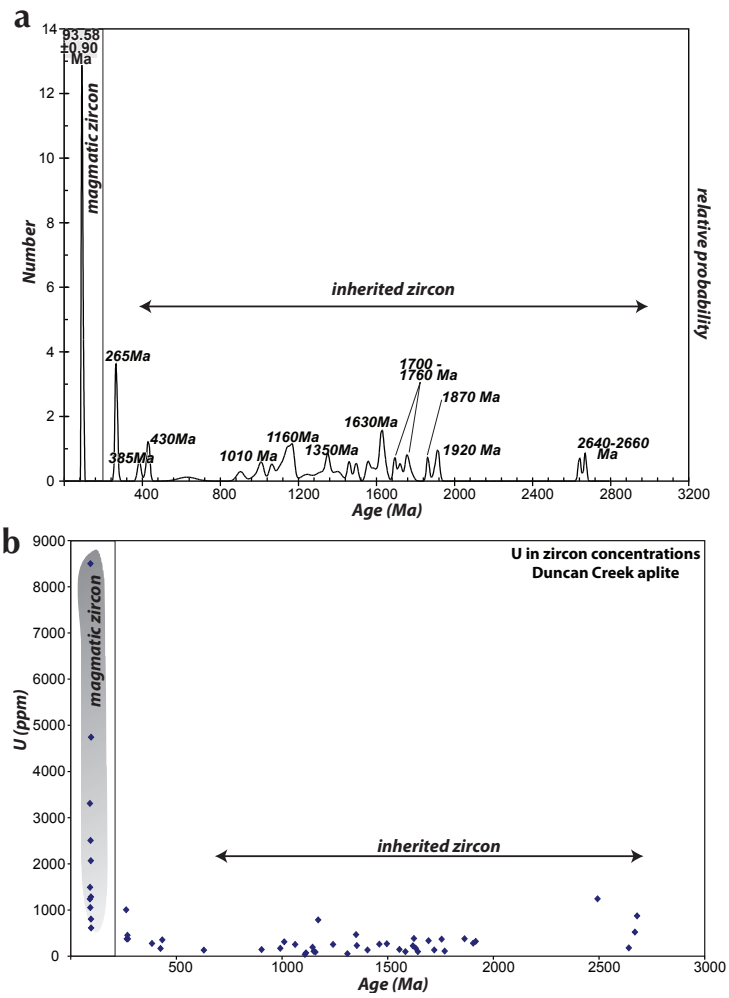

Figure 17. (a) *Cumulative-probability diagram illustrating the age distribution of inherited zircon populations within Duncan Creek aplite. Crystallization age plotted for reference and comparison to youngest inherited population.* ***(b)*** *U concentration vs.age for all zircon populations from the Duncan Creek aplite. Magmatic zircon is distinctive in high U concentrations when compared to the inherited populations (<1000 ppm).*

CONCLUSION

The integrated geological, geochemical, geophysical and geochronological datasets reported in this study for the Eagle Silver project highlight the presence of Tombstone-age intrusions and related structures that are more proximal to the Keno Hill silver veins than the Roop Lakes stock. Early-phase Ag-Pb-Zn mineralizing events recognized in the Eagle and Fisher veins are consistent with the polymetallic mineralization occurring in the historic adjacent veins and have an early bonanza-grade Au-enriched pyrite-marcasite-sphalerite ± cassiterite ± arsenopyrite phase associated with a quartz-siderite gangue (such as occurs at the Homestake occurrence); this phase of mineralization is overprinted by the more common sphalerite-galena-siderite veining. Petrographic evidence points to a complex paragenetic sequence during this intermediate stage of mineralization and also to the presence of at least two phases of siderite, pyrite and sphalerite mineralization. The prevalence of sphalerite over galena within the Eagle Vein may also directly reflect the elevated indium concentrations occurring within the Eagle Vein. The Eagle Vein is unique with respect to the occurrence of ubiquitous late-stage pyrite-pyrrhotite-arsenopyrite mineralization associated with low-grade gold concentrations, which occurs as replacement/skarn-like mineralization of weakly calcareous 'upper schist' host lithologies, and which also overprints earlier stage Ag-Pb-Zn mineralized veins. This style and grade of mineralization is more typical of Tombstone-age Au-As-W mineralization occurring elsewhere in the region (*e.g.*, Gold Dome, Dublin Gulch). The presence of *ca.* 93 Ma aplite dykes that occur at the periphery of an elongate, low-amplitude aeromagnetic high at the southeast end of Galena Hill is unique in the Keno Hill silver camp. The geometry of the anomaly is suggestive of a large buried intrusion that is bounded by several arcuate fault structures, including the McLeod-Fisher fault.

Collectively, the coincidence of *ca.* 93 Ma Tombstone-age intrusive bodies, unique late-stage mineralization and overprinting, low-grade Au-As mineralization within Ag-Pb-Zn veins and vein-faults occurring at the margins of, or within the defined extents of, a large, low-amplitude total magnetic intensity anomaly, in addition to Au-As replacement/skarn-like mineralization occurring at depth within the Eagle Vein fault system, imply that Tombstone-age intrusions postdate the prolific Keno Hill Ag-Pb-Zn mineralizing event, at least within the confines of the Eagle Silver project area.

ACKNOWLEDGEMENTS

Thank you to Mike Padula of Victoria Gold Corporation, Avino Silver and Gold Mines Ltd. and Mega Precious Metals Inc. for funding assistance for the analytical work. We thank Pam King, Earth Sciences Department, Memorial University and Michael Tubrett and Michael Schaeffer for access and assistance in the MafIIC analytical facility. Thank you to Don Murphy who reviewed and improved an earlier draft of the manuscript.

REFERENCES

Archer, A.R., 1979. Report on the recommended exploration, Keno Hill district. Internal report, Canada Tungsten Mining Corporation Ltd.

Beaudoin, G. and Sangster, D.E., 1992. A descriptive model for silver-lead-zinc veins in clastic metasedimentary terranes. Economic Geology, vol. 87, p. 1005-1021.

Becker, T.C., 2000. Assessment report describing prospecting, geological mapping, and soil geochemistry on the Fisher property. Assessment Report 09414, prepared for Expatriate Resources Ltd. by Archer, Cathro & Associates (1981) Ltd., 10 p.

Bennett, V. and Tubrett, M., 2010 (this volume). U-Pb isotopic age dating by LAM ICP-MS, INCO Innovation Centre, Memorial University: Sample preparation methodology and analytical techniques. *In:* Yukon Exploration and Geology 2009, K.E. MacFarlane, L.H. Weston and L.R. Blackburn (eds.), Yukon Geological Survey, p.47-55.

Bostock, H.S., 1947. Mayo, Yukon Territory. Geological Survey of Canada, Map 890A, scale 1:253,440.

Boyle, R.W., 1957. Geology and Geochemistry of the Silver Lead Zinc Deposits of Galena Hill, Yukon Territory. Geological Survey of Canada, Paper 57-1.

Boyle, R.W., 1965. Geology, geochemistry and origin of the lead-zinc-silver deposits of the Keno Hill-Galena Hill area, Yukon Territory. Geological Survey of Canada, Bulletin 111, 302 p.

Boyle, R.W., 1979. The geochemistry of gold and its deposits. Geological Survey of Canada, Bulletin 280, 584 p.

Boyle, R.W., Wanless, R.K. and Stevens, R.D., 1970. Sulfur isotope investigation of the lead-zinc-silver-cadmium deposits of the Keno Hill-Galena Hill area, Yukon, Canada. Economic Geology, vol. 65, p. 1-10.

Carmichael, A.D., Jr., 1957. United Keno Hill Mines. *In:* Structural Geology of Canadian Ore Deposits, Congress Volume, G. Gilbert, (ed.), Canadian Institute of Mining and Metallurgy, Geology Division, p. 66-77.

Cathro, R.J., 2006. Great mining camps of Canada: Announcing a new series. Geoscience Canada, vol. 33, no. 2, p. 56-59.

Cockfield, W.E., 1921. Silver-lead deposits of the Keno Hill area, Mayo District, Yukon. Geological Survey of Canada, Summary Report, 1920, Part A, p. 1-6.

Franzen, J.P., 1979. Metal-ratio zonation in the Keno Hill District. Unpublished paper presented at the Seventh Geoscience Forum, Whitehorse, Yukon.

Keller, D., Sedlacek, J., Doerksen, G., Ghaffari, H. and Lister, D., 2008. Bellekeno Technical Report, Keno Hill Mining District, Yukon. Alexco Resource Corp., June 30, SRK Consulting (Canada) Inc., 2008 <*http://sedar.com/CheckCode.do;jsessionid=0000SvE9Z_pRgPlvakhLU6NAaju:-1*> [accessed December 7, 2009].

Kindle, E.D., 1962. Geology, Keno Hill. Geological Survey of Canada, Map 1105A, scale 1:63,360.

Lebarge, W.R, Bond, J.D. and Hein, F.J., 2002. Placer gold deposits of the Mayo area, central Yukon. Exploration and Geological Services Division, Yukon Region, Indian and Northern Affairs Canada, Bulletin 13, 209 p.

LeBarge, W.P. (compiler), 2007. Yukon Placer Database 2007 - Geology and Mining Activity of Placer Occurrences. Yukon Geological Survey, CD-ROM.

Le Couter, P.C., 2009. Petrographic report on seven samples from the Eagle project, Galena Hill, Yukon. Unpublished internal report for MegaPrecious Metals.

Ludwig, K.R., 1999. User's manual for Isoplot/Ex, version 2.06: a geochronological toolkit for Microsoft Excel. Berkeley Geochronological Center, Special Publication No. 1a, 49 p.

Lynch, J.V.G., 1989. Large-scale hydrothermal zoning reflected in the tetrahedrite-freibergite solid solution, Keno Hill Ag-Pb-Zn district, Yukon. Canadian Mineralogist, vol. 27, p. 383-400.

Mair, J.L., Hart, C.J.R. and Stephens, J.R., 2006. Deformation history of the northwestern Selwyn Basin, Yukon, Canada: implications for orogen evolution and mid-Cretaceous magmatism. Geological Society of America Bulletin, vol. 118, p. 304-323.

McTaggart, K.C., 1960. The geology of Keno and Galena Hills, Yukon Territory. Geological Survey of Canada Bulletin 58, 37 p.

Mortensen, J.K. and Thompson, R.I., 1990. A U-Pb zircon-baddeleyite age for a differentiated mafic sill in the Ogilvie Mountains, west-central Yukon Territory. *In:* Radiogenic Age and Isotopic Studies, Report 3, Geological Survey of Canada, Paper 89-2, p. 23-28.

Murphy, D.C., 1997. Geology of the McQuesten River region, northern McQuesten and Mayo map areas, Yukon Territory (115P/14, 15, 16; 105M/13, 14). Exploration and Geological Services Division, Yukon Region, Indian and Northern Affairs Canada, Bulletin 6, 112 p.

Nelson, J. and Colpron, M., 2007. Tectonics and metallogeny of the British Columbia, Yukon, and Alaskan Cordillera, 1.8 Ga to the present. *In:* Mineral Deposits of Canada: A Synthesis of Major Deposit-Types, District Metallogeny, the Evolution of Geological Provinces, and Exploration Methods, W.D. Goodfellow (ed.), Geological Association of Canada, Mineral Deposits Division, Special Publication No. 5, p. 755-791.

Philpot, M.D., 1980. Geological and geochemical report; Bry mineral claims. Yukon Assessment Report 090545, prepared for Canada Tungsten Mining Corporation Ltd. by Bema Industries Ltd., 10 p.

Roots, C.F. and Murphy, D.C., 1992. New developments in the geology of Mayo map area, Yukon Territory. *In:* Current Research, Part A, Geological Survey of Canada, Paper 92-1A, p. 163-171.

Roots, C.F., 1997. Geology of the Mayo Map area, Yukon Territory (105M). Exploration and Geological Services Division, Yukon Region, Indian and Northern Affairs Canada, Bulletin 7, 82 p.

Sack, R.O., Lynch, J.V.G. and Foit, E., Jr., 2003. Fahlore as a petrogenetic indicator, Keno Hill Ag-Pb-Zn district, Yukon, Canada. Mineralogical Magazine, vol. 67, p. 1023-1038.

Scott, J. and Tupper, D.W., 2008. Mechanical trenching, rock, soil and stream sediment geochemical Assessment Report, Fisher 1-67 Claims. Unpublished assessment report.

Scriven, S., 2008. Report on a helicopter-borne magnetic gradiometer and VLF-EM, Fisher-Man Project. Unpublished internal report for MegaPrecious Metals.

Sinclair, A.J., Tessari, O.J. and Harakal, J.E., 1980. Age of Ag-Pb-Zn mineralization, Keno Hill-Galena Hill area, Yukon Territory. Canadian Journal of Earth Sciences, vol. 17, p. 1100-1103.

Tempelman-Kluit, D.J., 1970. The stratigraphy and structure of the "Keno Hill Quartzite"; in Tombstone River – Upper Klondike River map areas, Yukon Territory. Geological Survey of Canada, Bulletin 180, 102 p.

Tessari, O.J., 1979. Model ages and applied whole rock geochemistry of Ag-Pb-Zn veins, Keno Hill – Galena Hill mining camp, Yukon Territory. Unpublished MSc Thesis, University of British Columbia, Vancouver, British Columbia.

Thompson, R.I., Roots, C.F. and Mustard, P.S., 1990. Repeated Proterozoic passive margin extension influences Late Cretaceous folding and thrusting in southern Ogilvie Mountains, Yukon. *In:* Geological Association of Canada/Mineralogical Association of Canada, Program with Abstracts, vol. 15, p. A131.

Thompson, R.I., 1995. Geological compilation (1:250 000) map of the Dawson map area (116B, C; northeast of the Tintina Trench). Geological Survey of Canada, Open File 3223.

Watson, K.W., 1986. Ag-lead-zinc deposits of the Keno Hill – Galena Hill area, Yukon Territory. Yukon Geology, vol. 1, p. 83-88.

Appendix 1. *LAM ICP-MS U-Pb isotopic analyses of magmatic zircons from aplite dyke, D09-EF-05.*

	Measured isotopic ratios							Calculated ages										
Analysis	$^{207}Pb/^{235}U$	1σ err.	$^{206}Pb/^{238}U$	1σ err.	Rho	$^{207}Pb/^{206}Pb$	1σ err.	$^{207}Pb/^{235}U$ Ma	1σ err. Ma	$^{206}Pb/^{238}U$ Ma	1σ err. Ma	Conc. age (Ma)	2σ err. Ma	MSWD of conc.	Prob.	Th ppm	U ppm	Ratio Th/U
oc16a84	0.0977	0.0034	0.0145	0.0002	0.2391	0.0508	0.0017	95	3	93	2	93	3	0.28	0.60	108	3243	0.03
oc16b16	0.0973	0.0030	0.0145	0.0002	0.2359	0.0491	0.0017	94	3	93	1	93	3	0.34	0.56	117	4874	0.02
oc16b17	0.1035	0.0056	0.0144	0.0003	0.1634	0.0537	0.0014	100	5	92	2	93	3	2.31	0.13	131	4712	0.03
oc16b19	0.0998	0.0022	0.0148	0.0002	0.3079	0.0497	0.0012	97	2	95	1	95	2	0.64	0.42	85	4669	0.02

Appendix 2. *LAM ICP-MS U-Pb isotopic analyses of inherited zircons from aplite dyke, D09-EF-05.*

	Measured isotopic ratios							Calculated ages												
Inherited zircon	$^{207}Pb/^{235}U$	1σ err.	$^{206}Pb/^{238}U$	1σ err.	Rho	$^{207}Pb/^{206}Pb$	1σ err.	$^{207}Pb/^{235}U$	1σ err.	$^{206}Pb/^{238}U$	1σ err.	$^{207}Pb/^{206}Pb$	1σ err.	U-Pb/ Pb-Pb	Conc. age	2σ err.	MSWD of conc.	Prob. of conc.	Th ppm	U ppm	Ratio Th/U
oc16a73	2.1544	0.0633	0.1677	0.0033	0.3365	0.0937	0.0010	1166	20	1000	18	1502	21	67	1058	33	52.53	0.00	9	83	0.11
oc16a74	1.6897	0.0267	0.1675	0.0024	0.4546	0.0724	0.0004	1005	10	998	13	998	10	100	1003	19	0.26	0.61	9	937	0.01
oc16a75	0.5736	0.0220	0.0696	0.0016	0.2948	0.0599	0.0007	460	14	434	9	601	26	72	440	18	3.29	0.07	254	434	0.58
oc16a76	0.4802	0.0158	0.0644	0.0014	0.3220	0.0559	0.0004	398	11	402	8	447	17	90	401	15	0.13	0.72	311	654	0.47
oc16a77	13.4434	0.9066	0.4991	0.0356	0.5296	0.1976	0.0010	2711	64	2610	153	2806	8	93	2718	126	0.61	0.44	311	443	0.70
oc16a78	3.6684	0.1032	0.2781	0.0081	0.5177	0.0975	0.0011	1565	22	1582	41	1578	20	100	1565	45	0.24	0.63	57	164	0.35
oc16a79	4.5878	0.0692	0.3068	0.0038	0.4100	0.1076	0.0006	1747	13	1725	19	1759	10	98	1743	24	1.54	0.22	152	229	0.66
oc16a80	3.2641	0.0801	0.2377	0.0054	0.4643	0.0978	0.0005	1473	19	1375	28	1582	9	87	1454	38	14.57	0.00	159	414	0.38
oc16a81	2.8885	0.0483	0.2379	0.0036	0.4516	0.0877	0.0004	1379	13	1376	19	1375	8	100	1378	24	0.03	0.85	286	716	0.40
oc16a82	2.1770	0.0736	0.1961	0.0087	0.6541	0.0821	0.0009	1174	24	1154	47	1248	22	92	1176	46	0.30	0.59	354	705	0.50
oc16a83	4.5247	0.0835	0.3068	0.0054	0.4761	0.1057	0.0006	1736	15	1725	27	1726	10	100	1735	31	0.20	0.65	180	303	0.59
oc16a105	13.8985	0.4698	0.5596	0.0181	0.4793	0.1809	0.0010	2743	32	2865	75	2661	9	108	2739	64	3.37	0.07	29	88	0.33
oc16a109	10.8234	0.2183	0.4502	0.0087	0.4793	0.1697	0.0014	2508	19	2396	39	2554	14	94	2507	38	11.01	0.00	66	45	1.47
oc16a110	1.6131	0.0545	0.1612	0.0033	0.3034	0.0740	0.0010	975	21	964	18	1042	28	92	968	32	0.25	0.62	22	72	0.30
oc16a111	2.9213	0.0594	0.2317	0.0035	0.3664	0.0896	0.0007	1387	15	1344	18	1416	15	95	1370	28	5.32	0.02	36	136	0.26
oc16a112	3.3361	0.0831	0.2605	0.0053	0.4083	0.0914	0.0008	1490	19	1492	27	1455	18	103	1490	37	0.01	0.92	55	96	0.58
oc16a113	2.5353	0.0509	0.2071	0.0039	0.4743	0.0891	0.0004	1282	15	1213	21	1407	8	86	1268	29	13.05	0.00	135	698	0.19
oc16a114	6.2176	0.1031	0.3523	0.0056	0.4824	0.1234	0.0007	2007	15	1945	27	2006	11	97	2004	29	6.85	0.01	56	110	0.51
oc16a115	2.8896	0.1220	0.2388	0.0090	0.4483	0.0873	0.0007	1379	32	1380	47	1366	16	101	1379	62	0.00	0.98	40	130	0.31
oc16a116	5.4548	0.1098	0.3385	0.0064	0.4714	0.1166	0.0006	1894	17	1879	31	1905	9	99	1893	34	0.27	0.60	103	155	0.67
oc16a117	0.5745	0.0507	0.0747	0.0034	0.2610	0.0591	0.0008	461	33	464	21	572	31	81	464	39	0.01	0.92	60	175	0.35
oc16b18	5.6304	0.0760	0.3451	0.0044	0.4772	0.1201	0.0009	1921	12	1911	21	1958	14	98	1920	23	0.26	0.61	90	514	0.18

Appendix 3. *LAM ICP-MS U-Pb isotopic analyses of magmatic zircons from Duncan Creek aplite.*

	Measured isotopic ratios							Calculated ages										
Analysis	$^{207}Pb/^{235}U$	1σ err.	$^{206}Pb/^{238}U$	1σ err.	Rho	$^{207}Pb/^{206}Pb$	1σ err.	$^{207}Pb/^{235}U$ Ma	1σ err. Ma	$^{206}Pb/^{238}U$ Ma	1σ err. Ma	Conc. age (Ma)	2σ err. Ma	MSWD of conc.	Prob. of conc.	Th ppm	U ppm	Ratio Th/U
oc16b20	0.1098	0.0025	0.0146	0.0003	0.5098	0.0561	0.0013	105.8	2.3	93.5	2.2	99	4	31.16	0.00	179	8502	0.02
oc16b23	0.1000	0.0043	0.0143	0.0002	0.1548	0.0515	0.0024	96.8	4.0	91.7	1.2	92	2	1.60	0.21	542	1493	0.36
oc16b24	0.1004	0.0028	0.0151	0.0004	0.4408	0.0493	0.0011	97.2	2.6	96.6	2.3	97	4	0.05	0.82	110	4743	0.02
oc16b26	0.1018	0.0043	0.0145	0.0003	0.2567	0.0519	0.0018	98.4	3.9	92.6	2.0	93	4	2.18	0.14	301	1053	0.29
oc16b27	0.0972	0.0061	0.0150	0.0005	0.2457	0.0480	0.0029	94.2	5.6	96.0	2.9	96	6	0.10	0.75	335	612	0.55
oc16b28	0.0958	0.0050	0.0149	0.0004	0.2394	0.0484	0.0025	92.9	4.6	95.5	2.4	95	5	0.31	0.58	258	805	0.32
oc16b29	0.0948	0.0019	0.0147	0.0001	0.2013	0.0479	0.0009	92.0	1.8	94.0	0.7	94	1	1.26	0.26	1248	2507	0.50
oc16b30	0.0967	0.0026	0.0149	0.0002	0.3080	0.0487	0.0015	93.7	2.4	95.5	1.6	95	3	0.53	0.47	508	1284	0.40
oc16b31	0.0961	0.0041	0.0142	0.0003	0.2103	0.0498	0.0021	93.2	3.8	90.9	1.6	91	3	0.36	0.55	504	1240	0.41
oc16b33	0.0980	0.0036	0.0142	0.0003	0.2465	0.0510	0.0023	94.9	3.3	91.0	1.6	91	3	1.38	0.24	54	3307	0.02
oc16b34	0.0992	0.0044	0.0149	0.0003	0.2042	0.0491	0.0023	96.0	4.1	95.2	1.7	95	3	0.04	0.84	76	2067	0.04

Appendix 4. *LAM ICP-MS U-Pb isotopic analyses of inherited zircons, Duncan Creek aplite.*

	Measured isotopic ratios							Calculated ages													
Inherited zircon	$^{207}Pb/^{235}U$	1σ err.	$^{206}Pb/^{238}U$	1σ err.	Rho	$^{207}Pb/^{206}Pb$	1σ err.	$^{207}Pb/^{235}U$	1σ err.	$^{206}Pb/^{238}U$	1σ err.	$^{207}Pb/^{206}Pb$	1σ err.	U-Pb/ Pb-Pb	Conc. age	2σ err.	MSWD of conc.	Prob. of conc.	Th ppm	U ppm	Ratio Th/U
oc16b35	0.2968	0.0057	0.0415	0.0005	0.2865	0.0530	0.0010	264	4	262	3	331	42	79	263	5	0.11	0.73	322	1005	0.32
oc16b36	2.1128	0.0497	0.1939	0.0028	0.3040	0.0818	0.0011	1153	16	1142	15	1241	27	92	1147	25	0.33	0.56	56	255	0.22
oc16b37	0.3071	0.0093	0.0420	0.0010	0.4038	0.0532	0.0019	272	7	265	6	338	80	78	268	11	0.78	0.38	205	374	0.55
oc16b38	0.3024	0.0078	0.0428	0.0006	0.2763	0.0521	0.0017	268	6	270	4	290	76	93	270	7	0.10	0.75	202	374	0.54
oc16a21	2.7375	0.0703	0.2180	0.0040	0.3602	0.0847	0.0011	1339	19	1271	21	1309	24	97	1309	34	8.54	0.00	25	54	0.46
oc16a22	2.9909	0.0853	0.2437	0.0073	0.5278	0.0890	0.0009	1405	22	1406	38	1404	20	100	1405	43	0.00	0.98	46	136	0.34
oc16a23	4.6668	0.0742	0.2787	0.0045	0.5061	0.1174	0.0005	1761	13	1585	23	1917	8	83	1746	27	82.80	0.00	58	321	0.18
oc16a24	4.4203	0.0762	0.2937	0.0049	0.4828	0.1074	0.0006	1716	14	1660	24	1755	10	95	1711	28	6.93	0.01	119	368	0.32
oc16a25	5.1025	0.0869	0.3184	0.0050	0.4597	0.1166	0.0007	1837	14	1782	24	1904	11	94	1831	29	6.24	0.01	240	283	0.85
oc16a26	4.5344	0.0956	0.3098	0.0047	0.3563	0.1082	0.0009	1737	18	1740	23	1769	16	98	1738	32	0.01	0.93	44	111	0.39
oc16a27	4.4312	0.0697	0.3040	0.0040	0.4203	0.1053	0.0006	1718	13	1711	20	1720	10	99	1717	25	0.14	0.70	94	135	0.70
oc16a28	1.8904	0.0606	0.1907	0.0033	0.2733	0.0765	0.0011	1078	21	1125	18	1109	28	102	1106	31	4.03	0.04	34	40	0.85
oc16a29	1.5232	0.0309	0.1754	0.0044	0.6177	0.0722	0.0009	940	12	1042	24	991	26	105	931	25	28.06	0.00	55	170	0.32
oc16a30	1.8787	0.0496	0.1820	0.0028	0.2893	0.0767	0.0008	1074	17	1078	15	1113	20	97	1076	26	0.04	0.83	26	73	0.36
oc16a31	13.1906	0.7100	0.4988	0.0250	0.4657	0.1818	0.0007	2693	51	2609	108	2669	6	98	2693	102	0.80	0.37	218	522	0.42
oc16a32	1.8419	0.0276	0.1762	0.0024	0.4481	0.0748	0.0004	1061	10	1046	13	1062	12	99	1057	19	1.34	0.25	14	256	0.05
oc16a33	3.9167	0.0549	0.2814	0.0038	0.4832	0.1000	0.0005	1617	11	1598	19	1624	8	98	1616	23	1.25	0.26	272	386	0.71
oc16a34	2.7288	0.2228	0.2112	0.0139	0.4037	0.0867	0.0010	1336	61	1235	74	1354	22	91	1299	113	1.83	0.18	83	232	0.36
oc16a34	0.7709	0.2531	0.0884	0.0155	0.2674	0.0607	0.0013	580	145	546	92	630	45	87	553	173	0.05	0.82	47	131	0.36
oc16a40	4.2369	0.0431	0.2853	0.0033	0.5713	0.1038	0.0004	1681	8	1618	17	1693	7	96	1684	17	21.65	0.00	66	337	0.20
oc16a41	12.7988	0.2071	0.5135	0.0088	0.5297	0.1787	0.0008	2665	15	2672	37	2641	7	101	2665	30	0.04	0.84	165	181	0.91
oc16a42	3.3650	0.0561	0.2538	0.0033	0.3860	0.0964	0.0005	1496	13	1458	17	1556	10	94	1484	24	5.15	0.02	52	148	0.35
oc16a43	3.1670	0.0540	0.2483	0.0038	0.4475	0.0916	0.0004	1449	13	1430	20	1460	9	98	1446	26	1.13	0.29	47	261	0.18
oc16a44	0.5152	0.0218	0.0682	0.0016	0.2786	0.0565	0.0008	422	15	425	10	474	30	90	424	18	0.04	0.84	68	167	0.40
oc16a45	0.1500	0.0670	0.0150	0.0006	0.0475	0.1830	0.0069	142	59	96	4	2680	62	4	96	8	0.58	0.45	116	873	0.13
oc16a46	0.5135	0.0113	0.0695	0.0010	0.3329	0.0554	0.0005	421	8	433	6	430	21	101	429	11	2.36	0.12	223	354	0.63
oc16a47	0.3247	0.0162	0.0425	0.0012	0.2861	0.0539	0.0007	286	12	268	8	368	30	73	272	14	1.82	0.18	90	452	0.20

continued on next page

Appendix 4. *continued*

	Measured isotopic ratios							Calculated ages													
Inherited zircon	$^{207}Pb/^{235}U$	1σ err.	$^{206}Pb/^{238}U$	1σ err.	Rho	$^{207}Pb/^{206}Pb$	1σ err.	$^{207}Pb/^{235}U$	1σ err.	$^{206}Pb/^{238}U$	1σ err.	$^{207}Pb/^{206}Pb$	1σ err.	U-Pb/ Pb-Pb	Conc. age	2σ err.	MSWD of conc.	Prob. of conc.	Th ppm	U ppm	Ratio Th/U
oc16a48	0.3715	0.1699	0.0175	0.0047	0.2932	0.1636	0.0032	321	126	112	30	2493	33	4	107	59	2.43	0.12	38	1241	0.03
oc16a49	2.0841	0.0306	0.1896	0.0026	0.4719	0.0790	0.0004	1144	10	1119	14	1171	9	96	1139	19	3.54	0.06	246	787	0.31
oc16a50	4.7652	0.0561	0.3057	0.0029	0.3963	0.1140	0.0005	1779	10	1720	14	1863	7	92	1765	19	18.95	0.00	22	377	0.06
oc16a51	4.0743	0.0678	0.2892	0.0044	0.4551	0.0997	0.0008	1649	14	1637	22	1619	15	101	1648	27	0.35	0.55	77	227	0.34
oc16a52	3.9675	0.0673	0.2827	0.0038	0.3926	0.1010	0.0007	1628	14	1605	19	1642	13	98	1622	26	1.48	0.22	35	99	0.36
oc16a57	4.0333	0.0540	0.2837	0.0033	0.4376	0.1004	0.0006	1641	11	1610	17	1632	11	99	1636	21	4.07	0.04	114	174	0.66
oc16a58	0.4666	0.0169	0.0615	0.0015	0.3285	0.0563	0.0006	389	12	385	9	465	24	83	386	16	0.11	0.73	117	277	0.42
oc16a59	1.8066	0.0398	0.1857	0.0025	0.3050	0.0691	0.0006	1048	14	1098	14	903	19	122	1074	22	9.41	0.00	97	145	0.67
oc16a60	1.7363	0.0341	0.1715	0.0025	0.3687	0.0729	0.0005	1022	13	1020	14	1010	13	101	1021	22	0.01	0.91	94	312	0.30
oc16a61	2.0503	0.0374	0.1930	0.0027	0.3908	0.0779	0.0006	1132	12	1137	15	1144	14	99	1134	22	0.11	0.74	48	196	0.25
oc16a62	2.0541	0.0489	0.1954	0.0034	0.3694	0.0784	0.0007	1134	16	1151	19	1158	18	99	1140	28	0.76	0.38	29	90	0.33
oc16a63	3.4034	0.0541	0.2553	0.0037	0.4536	0.0934	0.0005	1505	12	1466	19	1496	10	98	1499	24	5.15	0.02	69	271	0.25
oc16a64	2.2555	0.0792	0.2046	0.0056	0.3902	0.0781	0.0008	1198	25	1200	30	1150	20	104	1199	45	0.00	0.96	52	109	0.48
oc16a65	2.7373	0.0412	0.2302	0.0030	0.4401	0.0865	0.0004	1339	11	1336	16	1350	10	99	1338	22	0.04	0.83	171	468	0.37
oc16a66	3.7721	0.0823	0.2764	0.0039	0.3236	0.0978	0.0008	1587	18	1573	20	1584	15	99	1581	30	0.38	0.54	46	99	0.47